Modeling the Gasification Process of Wood-Char Biomass

Niousha Mazaheri

Department of Bioresource Engineering

McGill University
Ste-Anne-de Bellevue, Quebec
November 2018

A thesis submitted to McGill University in partial fulfillment of the requirement for the degree of Master of Science

©Niousha Mazaheri, 2018

ACKNOWLEDGEMENTS

First and foremost, I would like to thank my supervisor, Prof. Abdolhamid Akbarzadeh for his kind and consistent support, incredible patience and guidance to help me every step of the research. In addition, I would like to thank Prof. Mark Lefsrud, my co-supervisor, for his insightful help and supervision to assist me through my Master thesis.

I also would like to thank Dr. Edris Madadian for his time and support for challenges I faced along the way, as well as my lab mates Armin Mirabolghasemi for his amazing help and making time while writing his own thesis, and Hamed Niknam, Shahin Eskandari, Jiahao Shi and Liang He which without their assistance and friendship this work would not have been possible.

I would like to send my gratitude to my parents, Dr. Mazaheri and Dr. Ghafoori whom I owe where I am today. Their warm-hearted and unlimited supports during my studies alongside my sibling Ali Mazaheri was the greatest motivation I could ever ask for.

Last but not least, I thank my beloved friends, Alban Delerue, Faezeh Bagherpoor, Holly Ammon, Yasaman Ezazi and Maria Nikolakakou for their incredible emotional support during my Master.

ABSTRACT

The importance of climate change and subsequently the necessity for sustainable energy production have been evident to researchers and experts in this field for the past decades. However, moving forward with increasing the industrialization of biofuels and replacing them with conventional fuels require persuading businesses with robust and vast research results on the benefits of biofuels. Implementing numerical modeling as preliminary tests for different biomass as well as analyzing the behavior of the system by changing the effective properties, provides a resourceful tool for experimentation and is financially beneficial. Gasification has become one of the most desirable thermochemical conversion processes in the clean energy production, specifically for the hydrogen gas, with the biomass being compatible with this conversion system as a feedstock. However, the complexity of this process and the high range of temperature limit the possible number of the experimental tests, leading to the lack of extensive experimental results in the literature for biomass gasification compared to the combustion process. As a result, computational modeling is an attractive alternative to fill the gap of knowledge on this matter.

This work consists of one extensive literature review on the numerical modeling of the gasification process and two numerical modeling that have the potential for better understanding of the gasification process in biomass feedstock. The first model provides effective thermal conductivity (ETC) of the wood-plastic composites (WPCs) by using a homogenization method implemented by a finite element method (FEM). The solid volume fraction and porosity is considered as parameters, and high-density polyethylene (HDPE) plastic and wood-char were the materials. The results showed improved ETC as the solid volume fraction increased and the polymer is added to the wood-char. The ETC is one of the most important properties that affect the thermal processes of gasification. Using the homogenization technique, we potentially can design the microstructure of feedstocks to optimize their performance when used in the gasification process. The second model is a 1D gasification model for a single particle in a downdraft gasifier. The 1D model considers reduction and oxidation reactions for char and provides temperature distribution along the radius and time. Temperature rapidly increases before reaching a steady state after 3000s. The temperature on the radiuses closer to the surface has a higher temperature compared to the core. The results were consistent with the analytical data and can be used to better understand the effect of porosity and thermal conductivity on temperature changes in feedstock during gasification.

RÉSUMÉ

L'importance du changement climatique et, subséquemment, la nécessité d'une production d'énergie durable ont été évidentes pour les chercheurs et les experts dans ce domaine au cours des dernières décennies. Cependant, pour industrialiser davantage les biocarburants et les remplacer par des carburants classiques, il faut convaincre les entreprises disposant de résultats de recherche solides et vastes sur les avantages des biocarburants. La mise en œuvre de la modélisation numérique en tant que tests préliminaires pour différentes biomasses, ainsi que l'analyse du comportement du système en modifiant les propriétés effectives, constituent un outil ingénieux pour l'expérimentation et sont financièrement rentables. La gazéification est devenue l'un des procédés de conversion thermochimique les plus recherchés dans la production d'énergie propre, en particulier pour l'hydrogène, la biomasse étant compatible avec ce système de conversion en tant que matière première. Cependant, la complexité de ce processus et la plage de température élevée limitent le nombre d'essais expérimentaux possibles, ce qui explique l'absence de résultats expérimentaux exhaustifs dans la littérature sur la gazéification de la biomasse par rapport au processus de combustion. En conséquence, la modélisation informatique est une alternative attrayante pour combler le manque de connaissances en la matière.

Ce travail consiste en une revue de la littérature approfondie sur la modélisation numérique du processus de gazéification et en deux modèles numériques susceptibles de permettre une meilleure compréhension du processus de gazéification de la biomasse. Le premier modèle fournit la conductivité thermique effective (ETC) des composites bois-plastique (WPC) en utilisant une méthode d'homogénéisation mise en œuvre par une méthode d'éléments finis (FEM). Les paramètres considérés étaient la fraction volumique solide, le plastique polyéthylène haute densité (PEHD) et le charbon de bois, ainsi que la porosité existante. Les résultats ont montré une amélioration de l'ETC à mesure que la fraction volumique solide augmente et que le polymère est ajouté au charbon de bois. L'ETC est l'une des propriétés les plus importantes des processus thermiques de gazéification. En utilisant la technique d'homogénéisation, nous pouvons potentiellement concevoir la microstructure des matières premières afin d'optimiser leurs performances lorsqu'elles sont utilisées dans le processus de gazéification. Le deuxième modèle est un modèle de gazéification 1D pour une seule particule dans un gazéifieur à évacuation descendante. Le modèle 1D prend en compte les réactions de réduction et d'oxydation du charbon

et fournit une distribution de la température le long du rayon et de la durée. La température augmente rapidement avant d'atteindre un état stable après 3000 s. La température sur les rayons les plus proches de la surface a une température supérieure à celle du noyau. Le résultat correspond aux données analytiques et peut être utilisé pour mieux comprendre l'effet de la porosité et de la conductivité thermique sur les changements de température dans la matière première pendant la gazéification.

Table of Contents

ACKNOWLEDGEMENTS	ii
ABSTRACT	iii
RÉSUMÉ	iv
Table of Contents	vi
Prefaces and Contribution of Authors.	viii
List of Abbreviations	ix
Nomenclature	xi
CHAPTER 1: Introduction	1
1. 3. Connecting statement	3
CHAPTER 2: Literature review	4
2. 1. Introduction	5
2. 2. Theoretical Basis of Gasification	6
2. 3. Advance Biofuels (Concentration in function of Biomass Properties in Canada)	20
2. 4. Optimization of Biomass Gasification Process	22
2. 5. Theoretical Modeling	27
2. 6. Concluding remarks	43
2. 7. Connecting statement	45
CHAPTER 3: Numerical homogenization model of effective thermal conductivity for wood- plastic composites	46
3. 1. Introduction	
3. 2. Methodology	
3. 2. 1 Model description	52
3. 2. 2 Solution Procedure	54
3. 3. Results and discussion	55
3. 4. Conclusions	59
3. 5. Connecting statement	60
CHAPTER 4: One-dimensional modeling of gasification in woody biomass particle	61
4. 1. Introduction	62

4. 2. Methodology	62
4. 3. Results and discussion	72
4. 4. Conclusions	74
Chapter 5: Summary and recommendation for future studies	75
References	77

Prefaces and Contribution of Authors

This thesis has been written in the manuscript-based format and consists of three articles. The first chapter is the literature review article which has been submitted to the Journal of Energy Conversion and Management. The next two articles will be submitted soon.

The literature review in the first chapter was researched and written by Niousha Mazaheri and Dr. Madadian. Prof. Akbarzadeh and Prof. Lefsrud reviewed, edited and proof-read the article.

The research for homogenization model of the second chapter was conducted and written by Niousha Mazaheri in collaboration with Armin Mirabolghasemi. The FEM calculation with ANSYS was performed with the great help of Armin Mirabolghasemi. Prof. Akbarzadeh and Prof. Lefsrud reviewed, edited and proof-read the chapter.

The gasification model of the third chapter was researched and written by Niousha Mazaheri. The model is developed based on an older version introduced by Dr. Dasappa. Prof. Akbarzadeh and Prof. Lefsrud reviewed, analyzed the results, edited and proof-read the article.

List of Abbreviations

1D one dimensional

CFD computational fluid dynamics

HHV high heating value

LHV low heating value

ER equivalence ratio

MC moisture content

db dry basis

CGE cold gas efficiency

HGE hot gas efficiency

MSW municipal solid waste

C&I commercial and industrial

SBR steam-to-biomass ratio

IGCC integrated gasification combined

cycle

FTS Fischer-Tropsch synthesis

CRF char reactivity factor

SCM shrinking core model

RPM random pore model

SEM scanning electron microscopy

MFD macroscopic fluid dynamics models

DEM discrete element model

DPM discrete phase model

WPC wood-plastic composites

ETC effective thermal conductivity

FEM finite element method

HDPE high density polyethylene

PE polyethylene

PP polypropylene

PVC polyvinyl chloride

PET polyethylene terephthalate

FVM finite volume method

FDM finite difference method

RVE representative volume element

UC unit cell

AEH asymptotic expansion

homogenization

Nomenclature

m_{wet}	Wet mass of the biomass	P_i	Partial pressure
m_{dry}	dry mass of the biomass	ψ	the effect of the porous structure of char
$oldsymbol{Q}_g$	the thermal energy of syngas, kJ/kg	S_{θ}	surface area
\dot{m}_g	gasification rate, kg/s	8 0	total volume
LHV _f	LHV of feedstock, kJ/kg	$L_{ heta}$	length of the porous
\dot{m}_f	feeding rate, kg/s	x_i	global length scales
T_f	the temperature of the feedstock	y_i	local length scales
T_0	reference temperature	χ_{j}	arbitrary characteristic function
m_H	mass fraction of hydrogen in solid fuel, kg	k_{ij}	conductivity tensor over the whole domain
h_{fg}	enthalpy of vaporization of water, kJ/kmol	Ω	Whole domain
X	the fractional carbon conversion	k_i	the thermal conductivity. i= w, p, a for wood-char, plastic and air
E	apparent pre- exponential constant	φ	the volume fraction of each phase

ρ	Density of gas phase, kg/m3	$Y_{i,s}$	Species concentration at gas film surrounded the particle surface
ρε	Density of non- porous wood char, kg/m3	$oldsymbol{Y_{i,\infty}}$	Species concentration at infinity
He	Calorific value of carbon	Le	Lewis number, $=\frac{\alpha}{D}$
rp	Pore radius, m	$oldsymbol{\dot{oldsymbol{arphi}}_{c}}'''$	volumetric char reaction rate term kg/(m3 s)
r	Radius, m	v	Fluid velocity, m
τ	Tortuosity factor	ṁ	Mass flow rate, kg/s
$\mathbf{k}_{\mathbf{c}}$	Non-porous char thermal conductivity	T	Temperature of radius r, K
$\mathbf{k}_{\mathbf{g}}$	Gas thermal conductivity	Ts	Particle surface temperature, K
k	Porous char conductivity	T_{∞}	Temperature at infinity, K
ϵ	Unreacted char porosity	De	Effective diffusivity, in porous media
C_p	Specific heat, kJ/(kg K)		
D	Diffusivity, (m ² /s)		

CHAPTER 1: Introduction

Water and food scarcity, greenhouse gas emissions and unsustainable conventional fuels are some of the critical issues which societies are facing around the world, and the researchers consider them as threats. However, governments still treat these issues as fictional and do not give the necessary support to achieve the required solutions. To challenge this kind of behavior and put more environmental-friendly projects in action, the researchers need to provide satisfactory evidence and studies supporting their hypothesis for the public that might not have the same knowledge on the subject. Numerical modeling provides such an interface by accelerating the process of research and providing unique insight on each issue.

Gasification is a complex process that produces valuable gases such as hydrogen from biomass, making it an attractive alternative to produce biofuels. The complexity of this process and a large number of fundamental parameters (e.g., gasifier characteristics and the feedstock physical and chemical properties) require a tool to be used simultaneously with the experiments. Numerical modeling is a fast, informative and accurate option for tackling this challenge. The objective of this thesis is to demonstrate the application of numerical modeling for the gasification process of biomass, as well as showing the advantages of modeling as an initial step that can replace needed experiments.

1. 2. Research problem

The research problem is to create two efficient numerical models to be used in different aspects of the gasification of biomass and consequently to produce biofuels from the gasification process.

1. 2. 1 Research objectives

The goal of this thesis is to use simple numerical modeling to define thermal characteristics of the complex process of gasification and demonstrate examples for implementation of this model, as well as introducing the application of the models. The sub-objectives can be written as:

• A thorough literature review has been carried out to outline the gasification modeling in the field of bioenergy production and fill the existing gap of knowledge in the

literature. This literature review has been written for the purpose of providing a guideline for any future modeling of gasification to help prevent unnecessary repetition in literature.

- Modeling the thermal conductivity, one of the essential thermal properties of the
 feedstock in the thermochemical process of gasification, by using the homogenization
 method to investigate the effect of effective thermal conductivity as well as the
 effectiveness of homogenization method for evaluating thermal properties of composite
 biomass including multiple phases.
- Developing a simple 1D modeling of the gasification of a single particle to examine the
 evolution of temperature in biomass for time and radius to help with understanding the
 gasification process at particle size. The model can be further implemented as a basis
 for 2D or 3D modeling in COMSOL.

1. 3. Connecting statement

Chapter 2 provides an extensive literature review on modeling the gasification process. The reactions, different types of gasifiers and modeling discussed. Examples of thermodynamics, kinetics and heat transfer modeling and their applications have been reviewed. The chapter is a proper guideline and background for understanding the following chapters.

CHAPTER 2: Literature review

Systematic Review of Research Guidelines for Numerical Simulation of Biomass Gasification for Bioenergy Production

N. Mazaheri¹, A.H. Akbarzadeh¹¹, E. Madadian^{1,2}, M. Lefsrud¹

Department of Bioresource Engineering, McGill University, Ste-Anne-de Bellevue, QC H9X 3V9, Canada

Department of Process Engineering and Applied Science, Dalhousie University, Halifax, NS B3H 4R2, Canada

Abstract

Sustainable energy production through conversion of biomass has recently found growing interest. Among thermochemical conversion techniques, gasification is of interest to replace direct combustion emitting air pollutants that threaten our environment. However, gasification process is still far from being efficient since most of the research studies have only focused on experimental implementation of the methods while numerical modeling has been limited to pilot scales, ignoring the performance optimization required for scaling up the gasification process. Gasification is a highly complex process, which involves the coupling of thermochemical equilibrium, kinetics, heat and mass transfer, and computational fluid dynamics. This complexity has currently prevented the proposed theoretical/computational models in the literature from achieving the required accuracy for optimizing the gasification process. Herein, we offer a comprehensive guideline to improve the numerical models which can be implemented in future sustainable biorefineries to improve their efficiency. The present study pursues two principal objectives: (1) Introducing the fundamental knowledge required for theoretical/computational modeling and (2) Reviewing alternative numerical models for the gasification process. First, a brief overview of the knowledge needed to make a systematic model is gathered. The theory of gasification, the various types of gasifiers and their differences are reviewed. Furthermore, we discuss the importance of the type of biomass feedstock with the concentration on advanced biofuels and focus on wood pellets for the modeling section. Second, CFD is introduced, and chemical equilibrium, kinetics, and heat and mass transfer models are discussed in depth, and the variation of different parameters concerning

the change of temperature within a gasifier is elaborated. The results of this study make a clear pathway for the modeling of the gasification process by anticipating the expected outputs from the model by using the existing experimental data. Finally, a comprehensive application of these models is demonstrated, and substantial parameters are affecting the gasification process such as biomass type and LHV are introduced. This review provides a framework for numerical modeling of the gasification process of biomass to optimize the efficiency of the conversion process.

2. 1. Introduction

With the increase of air pollution and greenhouse gas emission, production of biofuels has been introduced as a promising alternative to traditional fossil fuels. However, as a relatively new technology, there exist challenges that prohibit the industrial production of biofuels and the daily exploitation of bioenergy [1]. For example, most biofuels made of wood-based feedstocks have lower heating values and higher CO₂ emission than coal. This issue has created uncertainty over the sustainability of biofuels, disregarding their long-term benefits [2]. To clarify the misrepresentation of biofuels, researchers need to have a detailed evaluation of the applications of biofuels.

Properties of biofuels depend on the type of utilized biomass and the technology which has been used to produce it. Depending on the biofuel application and the origin of the feedstock used for the biorefinery, we can design an appropriate biofuel to meet our needs. For energy purposes, desirable biomass like wooden-based feedstock should have high heating value (HHV) and low inherent water content. Considering the HHV and water content as primary desirable properties of biomass for bioenergy production, Canada has one of the largest forestry industries in the world, and the by-products of this forestry industry are an excellent choice for biofuel production.

There have been various attempts to construct computer-based modeling for different biorefinery reactors to reduce the reliance on the experimental approaches and to have a financially and environmentally desirable biorefinery outcome. These computational models are based on thermochemical equilibrium, kinetic equation, heat and mass transfer, and computational fluid dynamics (CFD). Developing a computational model, which consider these mechanisms, provides a theoretical framework for tuning the parameters of the gasification process in order to optimize the thermochemical process for any specific biomass.

Over the past few years, there have been numerous studies on the modeling of biomass gasification [3]. In this paper, a guideline is developed for modeling of the gasification process. We review the rationale behind choosing each model and expected results. We have discussed the deficiencies of each model reviewed in this paper, while novel approaches are introduced to improve these deficiencies. The first part of this review paper elucidates the gasification theories, while the second part focuses on the existing models for the gasification process. Although there have been abundant works on both experimental and numerical modeling of biomass gasification, a systematic study to classify different steps of the gasification process is yet to be developed to be considered as a guideline for future works. Therefore, a general guideline which enables the researchers to evaluate the needs and procedure of conducting a gasification work is still in its infancy. The novelty of this study is presenting a road-map for future works on modeling gasification depending on the reactor type, type of biomass feedstock and operation parameters. Hence, the present work is extended to all cases and their different combinations. This study also covers the gaps in a variety of models in previous studies and suggests solutions to improve the accuracy of the theoretical/computational models.

2. 2. Theoretical Basis of Gasification

Gasification is one of the most effective energy conversion techniques for utilization of carbon-based feedstocks [4]. The design and operation of a gasifier require an understanding of the gasification process, gasifier configuration, gasifier size, feedstock size, feedstock characteristics, and the operating parameters of gasifier used for bioenergy production.

Gasification converts the carbonaceous feedstock into a gaseous fuel or chemical feedstock which can be further burned to release energy or can be used to produce value-added chemicals, e.g., hydrogen. Despite the relative similarity between gasification and combustion, they differ in the treatment of the product gas and the energy available within the chemical bonds in the product gas. The difference of combustion is in the release of the energy by breaking those chemical bonds [5]. The primary function of gasification is to produce gases with a high ratio of hydrogen to carbon by stripping carbon away from the hydrocarbon feedstock and by adding hydrogen. A conventional gasification process follows several successive steps: (1) Drying, (2) Pyrolysis, (3) Partial combustion of gasses, vapors, and char, and (4) Reduction of the combustion products.

Gasification, as one step after combustion, uses the reduction zone to make H₂ and CO from the combustion products. A clear understanding of each step of the gasification process is needed to model the thermochemical process accurately. In an ideal complete gasification process, the syngas only consists of CO and H₂. However, the ideal scenarios never take place due to reactions of the gasifying agent (air) and by-products (H₂O, CO₂, and CH₄), which exist from the pyrolysis and combustion processes.

2. 2. 1. Gasification medium and types of gasifying agents

A gasifying medium assists to break down the heavier solid hydrocarbons in order to convert them into low-molecular-weight gases like CO and H₂. There are a few well-known gasifying agents used in the process of biomass gasification, namely air, steam, oxygen, and carbon dioxide. The influence of using different agents on energy efficiency has been studied extensively in the literature [6-12]. For instance, Sharma et al. [6] conducted an experimental study on biomass gasification process in a downdraft reactor followed by saturated steam when the steady-state conditions achieved. They indicated that adding steam to air in the reduction zone increased the hydrogen flow rate. Ismail and El-Salam [7] studied air gasification of biomass in an updraft reactor and indicated that equivalence ratio, which is a function of both air and biomass, influenced the composition of synthesis gas. They concluded that the equivalence ratio has an indirect relation with the concentration of CO and H₂ while interacting directly with the CO₂ content of the gas.

The heating value and the composition of the gas products in a gasifier are dependent on the type and amount of the gasifying agent. A ternary diagram (Fig. 2.1) of carbon, hydrogen, and oxygen demonstrates the conversion path towards the formation of different gaseous products in a gasifier. Each corner of the triangle represents 100% of the element, and each point within the triangle is a mixture of the C, O, and H. Thus, each side of the triangle is divided into six parts to show the percentage available of elements. If oxygen is the gasifying agent, the conversion path moves toward the oxygen-driven reactions. In this case, the gasification products include CO with low amounts of oxygen and CO₂ for the high amount of oxygen. When the amount of oxygen exceeds the stoichiometric level, the process moves from gasification to combustion. The excessive air during the combustion results in producing flue gas which contains no residual heating value compared to fuel gas (or synthesis gas). If steam is the gasification agent, the process moves toward

the hydrogen-dominate reaction in Fig 2.1. The gas product contains more hydrogen per unit of carbon, resulting in a higher H/C ratio.

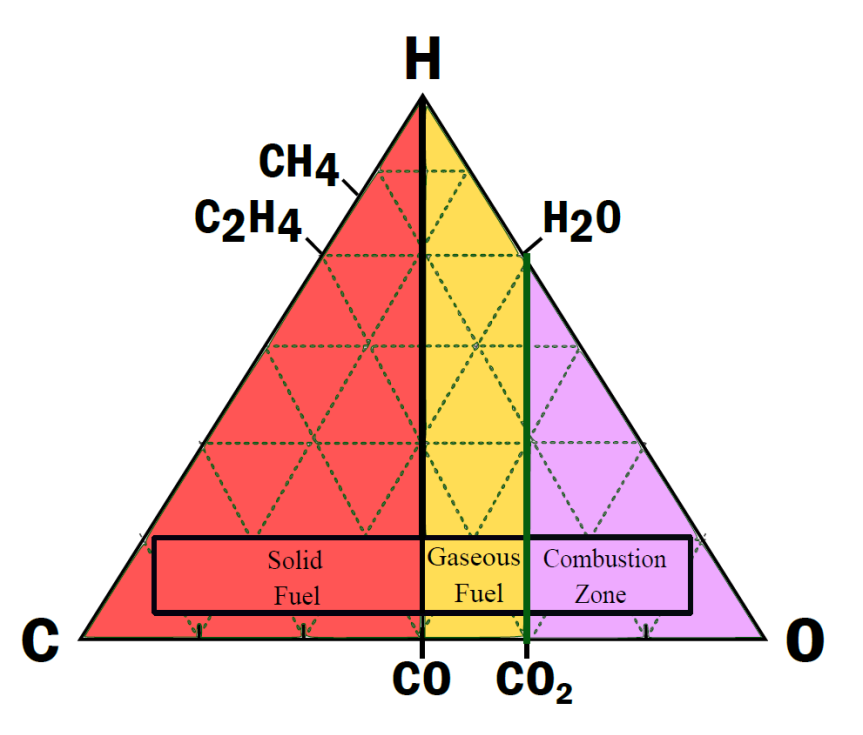


Figure 2.1: Ternary diagram of biomass showing the gasification process, where H and O represent hydrogen and oxygen [2]

Figure 2.2 shows the range of gasification products while using various gasifying agents [13]. As shown in Fig. 2.2, steam, as the gasifying agent, produces syngas with the highest H₂ content as well as a high content of CO and CO₂. Using air as the agent results in a higher production of CO and a lower amount of H₂ and CO₂, compared to a case when steam is used as the agent. The gasifying agent can also affect tar content in the char, syngas and equivalence ratio (ER) [14].

ER or the exact ratio of fuel to agent indicates the oxygen feed during gasification and presents a crucial parameter for the gasifier performance. The gasifier performance determines the range of syngas products. For example, Sharma et al. [6] reported that increasing ER decreases the molar fraction of nitrogen to a minimum value; afterward, an increase can be observed. In their experiment [6], the fraction of carbon monoxide and hydrogen shows an opposite trend to nitrogen when ER is increased. Carbon dioxide, however, monotonically increase by the increase of ER.

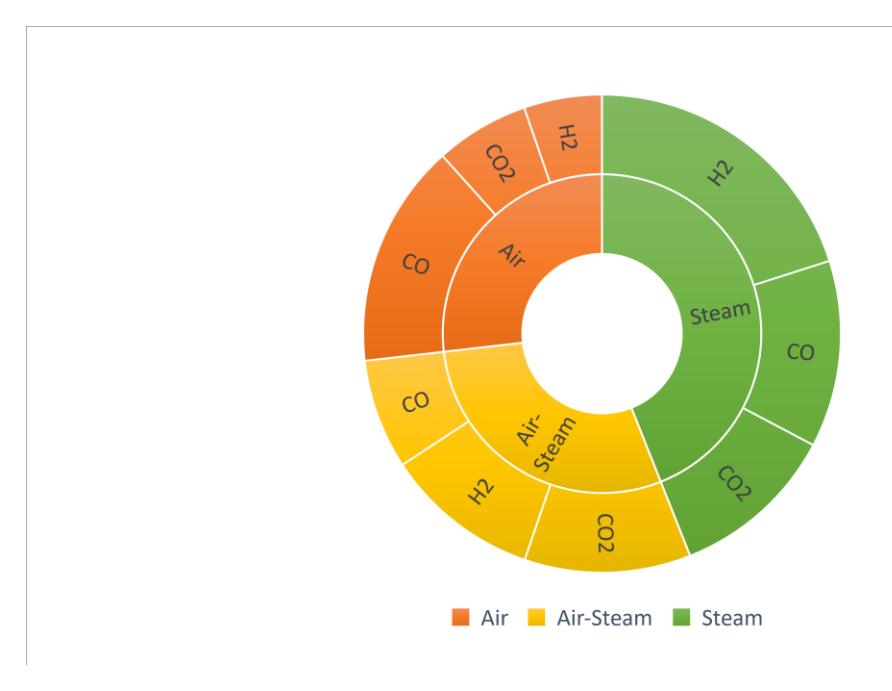


Figure 2.2: Effect of gasifying agents on the composition of gas products [13].

2. 2. 2. Types of gasifiers

There are several types of biorefinery reactors studied in the literature that impact the thermochemical conversion, e.g. updraft [7], downdraft [8, 15-17], cross-draft [18], fluidized bed [9, 19] and entrained flow gasifier [20] which fall into the three main categories: (1) moving (fixed) bed, and (2) fluidized bed and (3) entrained flow gasifier [21]. Moving bed and fluidized bed gasifiers are discussed here.

2.2. 2. 1. Moving bed gasifiers

Updraft gasifiers are the most straightforward configuration in moving bed reactors (Fig. 2.3.). In a conventional updraft gasifier, fuel is fed from the top, while the syngas leaves from the top. The gasifying agent (air, oxygen, steam, or their mixture) is pre-heated and fed into the gasifier through a grid at its bottom.

In a downdraft gasifier, biomass is fed from the top, while the entered gasification agent meets with the pyrolysis product, releasing heat (Fig. 2.3.). After that, both gas and solid (char and ash) products move down in the downdraft gasifier. Here, a part of the pyrolysis gas may burn above the gasification zone; this phenomenon, called as flaming pyrolysis, supplies the thermal energy required for the endothermic reactions through the combustion of pyrolysis gas [18, 22]. Drawbacks of a downdraft gasifier are namely grate blocking, channeling, and bridging which

hinder scaling-up the gasification process. The moisture content of feedstock in a downdraft gasifier should not exceed 30% to avoid inferior products and low efficiency [16]. A downdraft gasifier is beneficial for producing low-tar syngas and has a simple operation configuration. The syngas of a downdraft gasifier has less tar as well as lower LHV compared to an updraft [23].

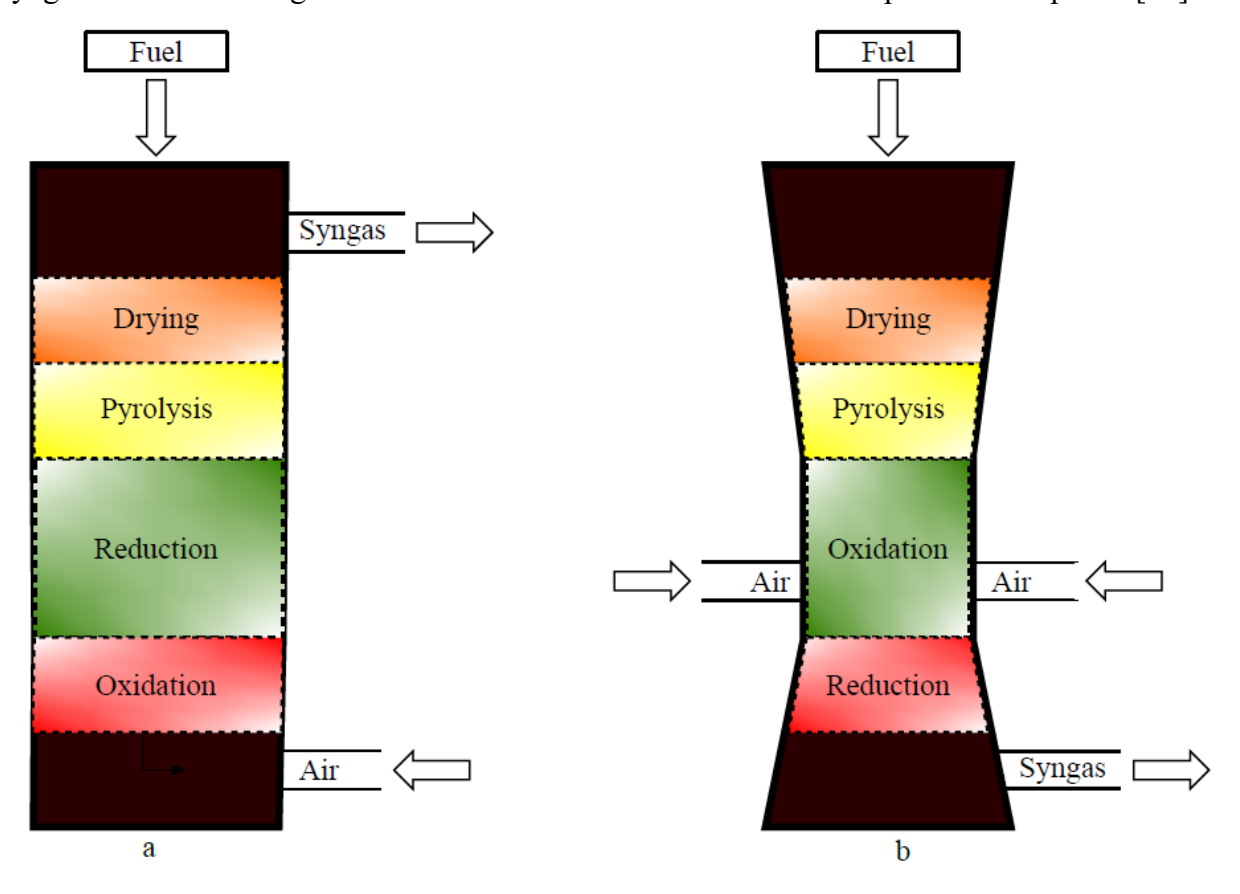


Figure 2.3.: Schematic diagram of (a) Updraft gasifier; and (b) Downdraft gasifier showing different stages of gasification

2. 2. 2. Fluidized bed gasifiers

Unlike other types of biorefinery reactors mentioned earlier, fluidized-bed gasifier contains non-fuel granular solids (bed solids) that act as a heat carrier and a mixer. The two types of fluidized bed are circulating fluidized bed and bubbling fluidized bed, differing in fluidization techniques [10]. In a bubbling fluidized bed, the fuel fed from either the top or the side is mixed quickly throughout the fluidized bed. The gasifying medium serves as the fluidizing gas and is sent through the bottom of the reactor, leading to a quicker mixture of fuel particles with the bed materials and thus much faster heating of the fuel. More rapid drying and pyrolysis processes occur in the bubbling fluidized bed gasifiers compared to the circulating type. A deficiency of this system as

stated by Ruiz et al. [23] is that partially gasified particles can exit the process as a result of mixing with gasified solids. The combustion reaction occurs in the fluidized phase resulting in a lower efficiency. Ruiz et al. [19] and Materazzi et al. [21] carry out an excellent comparison of different types of one stage gasifiers [11, 23] based on the parameters such as feed characteristics, temperature, and pressure. Mirmostaghimi et al. [24] studied the influential parameters on biomass conversion in a circulating fluidized bed gasifier and concluded that optimal gas production with lowest tar generation happened for the case of equivalence ratio 0.3 and biomass particle size and moisture content 3 mm and 9 wt%, respectively.

2. 2. 3. Gasification thermodynamics

Physical properties of fuel such as density [25, 26], thermal conductivity [25, 26] and diffusivity [27], affect its thermochemical conversion process. Some of the main properties that have been commonly used in the literature are explained in the following.

2. 2. 3. 1. Moisture expression

Researchers often express biomass moisture content (MC) on a dry basis (db). Siau et al. define the dry basis MC (MC_{dry}) as [12]:

$$MC_{dry} = \frac{m_{wet} - m_{dry}}{m_{dry}} \tag{2.1}$$

where m_{wet} and m_{dry} are the wet and dry mass of the biomass respectively. This definition may give a moisture percentage greater than 100% for very wet biomass. Similarly, the wet basis MC (MC_{wet}), is defined as:

$$MC_{wet} = \frac{m_{wet} - m_{dry}}{m_{wet}} \tag{2.2}$$

Considering the importance of the MC on the gasification, this parameter is usually determined using the portable measuring devices on site. Based on the type of these devices, the MC can be wet-based or dry-based [28], and equation (2.3) can be used for the conversion:

$$MC_{dry} = \frac{MC_{wet}}{1 - MC_{wet}} \tag{2.3}$$

Rico-Contreras et al. [29] studied the poultry litter combustion to test the feasibility of this type of biomass. The fuzzy logic was used to predict the MC and the Monte Carlo simulation for the stability of the system. Here the MC for experimentation conditions is defined in dry basis as

equation (2.1). McKeown [30] designed a microwave system to predict the MC in the flowing bulk material and determine the feasibility of the system compared to the static calculations as well as reference data. The reference moisture here is calculated on the wet-basis using equation (2.2). Xin et al. [31] investigate the effect of MC and the temperature on the quality of syngas for the cattle manure, as well as the char characteristics. Here, the wet-based MC equation (2.2) was used in reverse to calculate m_{wet} for the sample.

2. 2. 3. 2. Biomass composition

There are three methods of expressing biomass composition for the description of experiments. In Figure 2.4, we have used the data for wood pellets composition from proximate analysis by Madadian et al. [25] and showed the different methods:

- (1) **As-received**: Containing everything in the fuel
- (2) Air-dry: When the surface of the fuel is dried, but inherent moisture remains
- (3) Dry: When thoroughly dried out

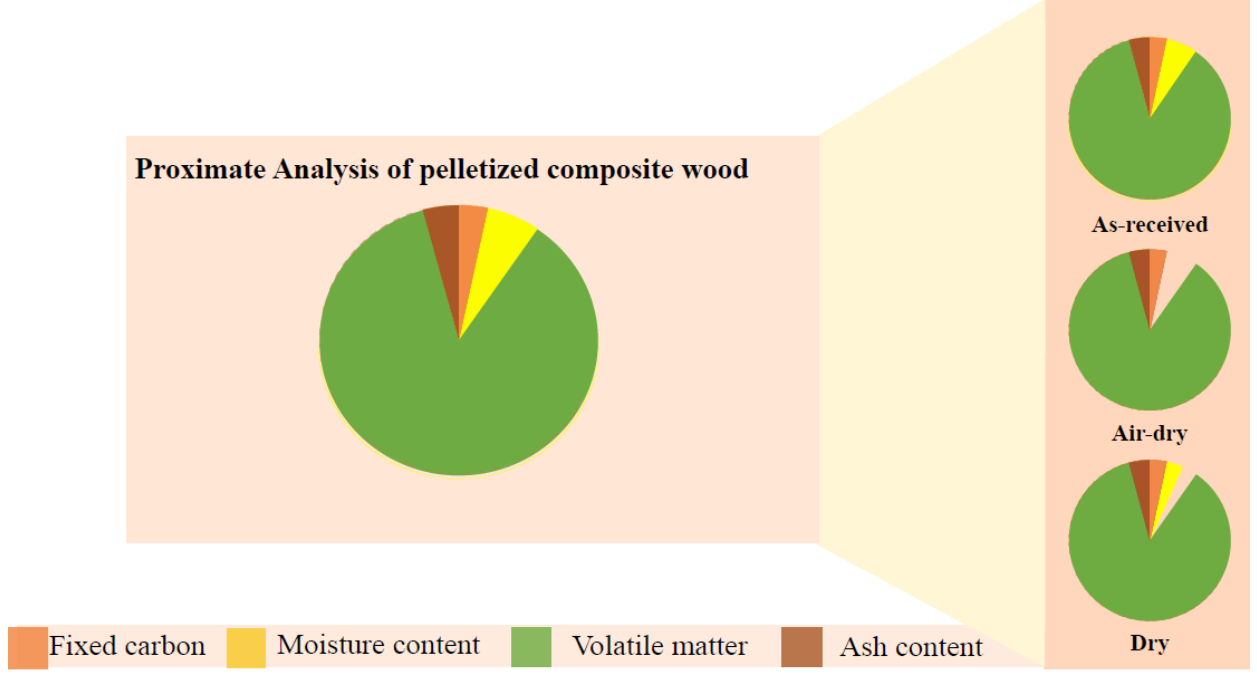


Figure 2.4: Three main biomass composition expressions based on proximate analysis: As received, Air-dry and dry. The data used for proximate analysis has been taken from reference [25].

2. 2. 3. 3. Gasification efficiency

The literature expresses the efficiency of the gasification process regarding the syngas specifications. Here, three leading indicators of the syngas quality are defined as follows:

(1) Cold gas efficiency: For cold gas efficiency (CGE), the high temperature of syngas leaving the system is not considered and therefore it is called CGE. The CGE term is denoted by η_{cg} and can be applied for the gasification processes where the syngas is cooled down before entering the energy production system [32]:

$$\eta_{cg} = \frac{\text{syngas thermal energy leaving the gasifyer [MW]}}{\text{feedstock thermal energy entering the gasifier [MW]}} = \frac{Q_g \dot{m}_g}{\text{LHV}_f \dot{m}_f} \times 100\% \tag{2.4}$$

where Q_g is thermal energy of syngas (kJ/kg), \dot{m}_g is gasification rate (kg/s), LHV_f is LHV of feedstock (kJ/kg) and \dot{m}_f is feeding rate (kg/s).

(2) **Hot gas efficiency**: For special cases, such as direct combustion, that the cooling down of the syngas is not necessary, the sensible heat of the gas is added for syngas thermal energy and efficiency is calculated as hot gas efficiency (HGE):

$$\eta_{hg} = \frac{Q_g \dot{m}_g + M_g C_p (T_f - T_0)}{LH V_f \dot{m}_f}$$
 (2.5)

where T_f is the temperature of feedstock and T_0 is reference temperature.

(3) Lower Heating Value: The lower heating value (LHV) is defined as the heat released by complete fuel combustion if the syngas temperature has not dropped down to the room temperature. On the contrary, the higher heating value (HHV) considers the syngas temperature value back to room temperature, thus releasing the energy of water condensation as a part of the heating value of the fuel. HHV is calculated based on the chemical composition of solid waste on the dry ash-free basis, and consequently, LHV can be calculated by removing the amount of the latent heat of vaporization [33]:

$$LHV = HHV - 9m_H h_{fg} (2.6)$$

where m_H is the mass fraction of hydrogen in solid fuel (kg) and h_{fg} is enthalpy of vaporization of water, (kJ/kmol).

Table 2.1 demonstrates the interaction relation between different types of gasifiers, biomass, and efficiency indicators. Wood-based pellets have higher heating value and lower moisture content among all types of biomass and therefore are one of the most popular biomasses used as a feedstock [34]. Besides, blending the biomass feedstocks can potentially enhance the energy density of the biomass and foster the efficiency of the gasification process. Madadian et al. [25, 26, 35, 36] reported studies on the gasification of fiber and plastics derived from municipal solid waste streams. They analyzed the thermal, chemical and mechanical specifications of the blends of fiber and plastics in the form of composite pellets and then investigated their thermomechanical conversion process.

Materazzi et al. [11] implemented a fluidized-bed gasifier using a mixture of automotive shredder residue and municipal solid waste (MSW) (1:1 ratio) which resulted in syngas with 17.68 MJ kg⁻¹ LHV and 0.8 CGE. Similarly, refuse-derived-fuel from (landfill mine waste) resulted in 21.91 MJ kg⁻¹ and 0.83 for the LHV and the CGE, respectively. For the same gasifier, using a mixture of MSW and commercial and industrial (C&I) wastes led to LHV of 16.8 MJ kg⁻¹ and CGE of 0.8. In these three cases, the higher carbon content of the raw material, as well as the desired performance of the reactor, results in high efficiency of the process. For example, Jarungthammachote et al. [33] implemented data from 9 different runs for a downdraft gasifier and wood rubber as feedstock to model the gasification resulting in 3.92 MJ kg⁻¹ of LHV and 0.19 of CGE. Table 2.1 gives a summary of different research conducted on gasification of a variety of feedstock.

Sepe et al. [37] developed a kinetics model by using a solar assisted gasification process to supply the required heat of the endothermic reactions during the thermochemical conversion of biomass in the gasifier. The value of LHV and CGE syngas was measured as 17.5 MJ kg⁻¹ and 1.25, respectively; these values are higher than the maximum performance of the high-temperature steam gasification, i.e., LHV of 13 MJ kg⁻¹ and CGE of 0.93 [37]. Comparing the two recent cases indicated lower efficiency for the process operated with air compared to the steam gasification.

Table 2.1: LHV and CGE of different type of biomass.

Reference No.	Biomass type	Model type	Syngas LHV (MJ/kg)	CG E
A (0.25% plastic)	Mixed Wood pellets	Thermodynamic	19.88	0.9
[38]	/ SLF-plastics	(Dual fluidized bed)		
B (0.5% plastic) [38]	Mixed Wood pellets / SLF-plastics	Thermodynamic	19.88	0.7
C (0.755 plastic) [38]	Mixed Wood pellets / SLF-plastics	Thermodynamic	19.88	0.6
(case 1) [11]	50% automotive shredder residue (ASR) and 50% MSW	Thermodynamic (Fluidized bed)	17.68	0.8
(case 2) [11]	Landfill mined waste (RDF)	Thermodynamic	21.91	0.8
(case 3) [11]	50% MSW and 50% commercial and industrial (C&I) wastes	Thermodynamic	16.80	0.8
[33]	Nine experimental data reported	Thermodynamic (Downdraft gasifier)	3.92	0.2
(Autothermal- steam gasification) [37]	Unknown	Kinetics (High power packed-bed reactor)	9.95	0.7
(High-temperature air gasification) [37]	Unknown	Kinetics	10.27	0.7
(High-temperature steam gasification) [37]	Unknown	Kinetics	13	0.9
(Solar assisted gasification) [37]	Unknown	Kinetics	17.50	1.2
(A1) [34]	Wood particles	Heat transfer (Fluidized bed)	8.48	0.5

The gasification process can be implemented either autothermally or allothermally [39]. In the former scenario, the energy required for gasification is obtained by the partial oxidation of the raw

material, while an externally heated source is feeding the allothermal gasifier. The comparison concludes that the allothermal gasification process is more efficient concerning thermal energy than the autothermal type. The reason can be the external heat source which aids the exothermic reactions of the process to supply enough power to run the endothermic reactions.

To improve the LHV and CGE of the produced gas during gasification, one should identify the main parameters controlling either the heating values of biomass or syngas. The composition of biomass and syngas are principle factors restraining the result of the gasification process. Ideal biomass for gasification has a high carbon content and low ash and moisture contents. The carbon content determines the gap between the experimental data and the equilibrium models [40], i.e., high carbon content directs a model closer to an equilibrium state resulting in reproducing an ideal syngas [41]. On the contrary, high ash content is detrimental and keeps the process away from reaching equilibrium. Furthermore, one of the main characteristics of biomass is the MC. By increasing the MC, the gasification process requires more heat to evaporate the moisture [8]. Subsequently, lower values of heat are available to raise the temperature of the gasifier resulting in a syngas with inferior quality (lower concentration of the H₂ and CO and reduced LHV of the syngas) [10].

The size of pellets manufactured from biomass is another parameter affecting the gasification process and consequently the quality of produced syngas. The main issue reported with increasing pellet's diameter is reducing the contents of hydrogen and carbon monoxide, which reduces LHV [42]. Masmoudi et al. [42] further discuss the trade-off effects of pellet size, where small particle creates a non-homogenous distribution of the gas flow in the bed by reducing the pressure inside the biorefinery reactor. As a result, selecting an appropriate size for feedstocks is vital for the efficiency of their thermo-chemical conversion process [43]. There are additional elements that play crucial roles in enhancing the LHV of syngas. One of the most important parameters is the process temperature.

The Le Chatelier's principle states that temperature increase can advance the reactions toward the products (Boudouard reaction, water–gas reaction, and steam-methane reforming reaction) or reverse the direction of the reaction (methanation reaction and CO shift reaction) [44]. Increasing temperature will increase the H₂ concentration and light hydrocarbon gases while the amount of the CH₄ and the CO₂ decreases in a specific temperature range [41]. For example, Ismail et al. [7]

reported 350 °C to 850 °C as the temperature range that he observed an increase for the H₂ and the CO. As a result, by increasing temperature, a remarkable growth for the LHV and the gas yield occurs.

Another vital factor for heating value of biomass is the steam-to-biomass ratio (SBR). Char gasification and water-gas shift reactions show improvement when SBR increases leading to the LHV increase [13]. However, there is an optimum SBR which in some cases Sepe et al. report as one [37]. For SBRs greater than the optimum value, the water-gas shift reaction can have a higher rate of reaction than desired. Meanwhile, the steam absorbs heat causing temperature reduction restricting other reactions. The temperature reduction leads to the overaccumulation of CO₂ resulting in inferior syngas production along with the reduced gas yield. Furthermore, the gasifier temperature controls the optimum SBR and needs to be considered while determining the preferred SBR for increasing LHV [10].

Additionally, the ER is a parameter influencing the LHV of the syngas. It is recommended to keep ER relatively low to enhance the syngas quality [13]. Nonetheless, the literature has introduced two different aspects of the influence of the ER on LHV [7, 10]. Increasing the ER results in further combustion creating a greater thermal heat and LHV is improved. In contrast, additional combustion absorbs the combustible gases affecting the syngas components. Therefore, estimating the optimum value of ER is necessary.

As gasification technology improves, scientists introduce additional modifications, for example, addition of CO₂ absorbent [13], reducing the rate of heat [10], increasing the operating pressure [3], lowering the bed height [3], increasing the airflow rate [7] and intensifying the concentration of oxygen in air [10] have been reported to be useful for improving the LHV and the yield of the syngas in the gasification process.

2. 2. 4. Gasification kinetics

The processing time of char gasification is much higher than the pyrolysis process which produces the char. Thus, the volume of a gasifier chamber is more dependent on the rate of the char gasification than the pyrolysis process. The gasification process contains three main gas-solid and one gaseous phase reactions as follows:

2. 2. 4. 1 Gas-solid reaction

The typical temperature of the gasification zone in the downdraft and fluidized-bed reactors is in the range of 700-900°C. The three most common gas-solid reactions that occur in the char gasification zone are [44]:

1- Boudouard reaction: R1:
$$C + CO_2 \rightarrow 2CO$$
 (2.7)

2- Water-gas reaction: R2:
$$C + H_2O \leftrightarrow CO + H_2$$
 (2.8)

3- Methanation reaction:
$$R3:C + 2H_2 \leftrightarrow CH_4$$
 (2.9)

For the air or oxygen gasifiers, the Boudouard reaction *R1* is the governing reaction, while the water-gas reaction R2 is the dominant reaction in steam gasifiers.

A simplified form of gas-solid char reaction, r, is the n^{th} -order expression [45]:

$$r = \frac{1}{(1-X)^m} \frac{dX}{dt} = A_0 e^{-E/RT} P_i^n$$
 (2.10)

where X is the fractional carbon conversion ($\frac{\text{moles of reactant that has reacted}}{\text{moles of reactant fed in}}$), A_0 is the apparent pre-exponential constant, E is the activation energy, T is the temperature of reaction in Kelvin, T0 and T1 are the reaction orders, considering the carbon conversion and gas partial pressure T2 respectively.

Boudouard Reaction: an excellent model for the rate of Boudouard reaction is known as the Langmuir-Hinshelwood rate [46] which considers CO inhibition to express the apparent gasification reaction rate, r_b as:

$$r_b = \frac{k_{b_1} P_{CO_2}}{1 + \left(\frac{k_{b_2}}{k_{b_3}}\right) P_{CO} + \left(\frac{k_{b_1}}{k_{b_3}}\right) P_{CO_2}}$$
(2.11)

where P_{CO} and P_{CO_2} are the partial pressures of CO and CO₂ on the char surface, respectively. The rate constants k_{b_i} are given in the form of $A_i \exp(-\frac{E_i}{RT})$. Barrio and Hustad [47] defined Boudouard reaction rate by using the widely accepted char gasification reaction with CO₂ which can be represented by the following reaction path:

$$C_f + CO_2 \underset{k_{1b}}{\overset{k_{1f}}{\longleftrightarrow}} C(O) + CO \tag{2.12}$$

$$C(O) \stackrel{k_3}{\to} CO \tag{2.13}$$

where C_f is an available active site, and C(0) is an occupied side, so-called as carbon-oxygen complex, or a transitional surface oxide. They modeled the rate of the reaction as:

$$r(T, P_{CO_2}, P_{CO}, X) = r_c(T, P_{CO_2}, P_{CO}) \times f(X)$$
(2.14)

where f(X) is called *structural profile*. Therefore, the function r_c does not depend on the degree of conversion. A 6th order polynomial represents this structural profile:

$$f(X) = A_0 + A_1 X + \dots + A_6 X^6 \tag{2.15}$$

where curve fittings result in coefficients A_0 to A_6 . The function f(X) is normalized by the value of the reaction rate at X = 0.5 so that f = 1 at 50% conversion rate. Equation (2.16) gives the degree of conversion X:

$$X = 1 - \frac{m(t) - m_f}{m_0 - m_f} \tag{2.16}$$

where m(t) is the mass of remaining biomass at time t, m_f is mass of tar at the end of gasification at gasification temperature (gaseous). The equation (2.17) defines reactivity as:

$$r = -\frac{1}{m(t) - m_f} \frac{d(m(t) - m_f)}{dt} \tag{2.17}$$

or regarding the degree of conversion as:

$$r = \frac{1}{1 - X} \frac{dX}{dt} \tag{2.18}$$

Langmuir-Honshelwood kinetics and steady-state assumption for CO, define the reaction rate as:

$$r_{c} = \frac{k_{1f} P_{CO_{2}}}{1 + \left(\frac{k_{1b}}{k_{3}}\right) P_{CO} + \left(\frac{k_{1f}}{k_{3}}\right) P_{CO_{2}}}$$
(2.19)

Equation (2.20) further simplifies Eq. (2.19):

$$r_{c} = \frac{k_{3}}{1 + (\frac{k_{1b}}{k_{1f}}) \frac{P_{CO}}{P_{CO_{2}}}}$$
(2.20)

which means that the reaction rate depends only on the ratio P_{CO}/P_{CO_2} and not the partial pressures.

Water-Gas Reaction: the equation (2.21) determines water-gas reaction as

$$C + H_2O \leftrightarrow CO + H_2 \tag{2.21}$$

This reaction rate can be written in the Langmuir-Hinshelwood form to consider the inhibition effect of the hydrogen and the other complexes [10]:

$$r_{w} = \frac{k_{1f} P_{H_{2}O}}{1 + \left(\frac{k_{1f}}{k_{3}}\right) P_{H_{2}O} + \left(\frac{k_{1b}}{k_{3}}\right) P_{H_{2}}}$$
(2.22)

where k_{w_i} are the reaction rates of the following reactions respectively:

$$C_f + H_2 O \underset{k_{1h}}{\overset{k_{1f}}{\longleftrightarrow}} C(O) + H_2 \tag{2.23}$$

$$C(0) \stackrel{k_3}{\to} C0 \tag{2.24}$$

Methanation (Hydrogasification) Reaction: methanation or hydrogasification is the conversion of the char into the methane by the addition of the hydrogen in a chemical reaction as:

$$C + 2H_2 \leftrightarrow 2CH_4 \tag{2.25}$$

This reaction shows rapid progress at the beginning of gasification but slows down significantly due to graphitization of the carbon. This reaction results in a substantial volume change and therefore will be highly sensitive to pressure.

2. 2. 4. 2. Gaseous Reactions

Among various gaseous phase reactions, the most important one may be the *Water-gas Shift Reaction*:

$$CO + H_2O \leftrightarrow CO_2 + H_2 \tag{2.26}$$

This reaction is exothermic, i.e. $\dot{Q} = -41 \, kJ/mol$, and the volume does not change significantly. Therefore, this process is almost insensitive to the pressure change. The equilibrium yield decreases as the temperature is increased as opposed to the reaction rate which increases. Therefore, to obtain equilibrium yields and high reaction rates, for a catalyst is needed.

2. 3. Advance Biofuels (Concentration in function of Biomass Properties in Canada)

Over the past few decades, the utilization of biofuel as a replacement for fossil fuels has become gradually popular resulting in their transformation from research-based applications to

industrializing the biofuel usage. However, the industry still faces considerable challenges in commercializing biofuels.

Biomass can be defined as any material with biological origin excluding the material embedded in geological formations and transformed into fossil [48, 49]. Biofuel is a product of biomass which can be used as a fuel in a variety of forms such as solid, liquid or gas to produce energy. Depending on their origin, biofuel is divided into two types, namely as: (1) conventional or first generation and (2) advanced or second/third/fourth generation.

The first-generation biofuels are extracted from food feedstocks creating a competition for the food industries, whereas advanced biofuels have relatively sustainable sources without implementing food feedstocks. Most of the first-generation fuels have already been commercialized, and they have been proved to be a cheap and feasible replacement for fossil fuels which results in lower prices. However, advanced biofuels are still in a pilot stage which requires further research to be used in industrial scale for sustainable energy production. This gap is an undesirable factor that encourages investors towards conventional biofuels, regardless of the long-term benefits of advanced biofuels.

The geographical location of biomass plays a significant role in how a specific biofuel is beneficial and sustainable. For example, for a developing country with inadequate sewage treatment systems, using sewage as a feedstock for biofuel is beneficial. Whereas for a country with great forestry resources, using the by-products of existing forestry industries enhances the sustainability. For countries that produced conventional biofuels such as bioethanol as one of the essential fuels, an effort is required to convert the feedstock of bioethanol from conventional biofuels to an advanced type. Means for biomass transportation required pre-treatment process of biomass, and the type and size of biorefinery reactors used for bioenergy production are among the other concerns that should be considered [50].

Another critical factor is the feedstock type affecting carbon content of biofuel and required treatment for conversion of biomass to biofuel, both changing the gasification process and the syngas quality. Figure 2.5 compares the ash and carbon content of a few different types of biomass [11, 51-56]. This figure provides a rough comparison between different types of biomass. LHV plays a more significant role than carbon content for comparison of different kinds of biomass.

In this paper, we focus on woody biomass due to its low ash content compared to the other types of biomass and because of its preferable carbon content. According to Natural Resources Canada [57], Canada holds the position for the world's most substantial forest production trade balance. This position shows the extent of the forestry industry in Canada revealing that how using second or third generation wood by-products can be beneficial for increasing sustainability for this large trade product.

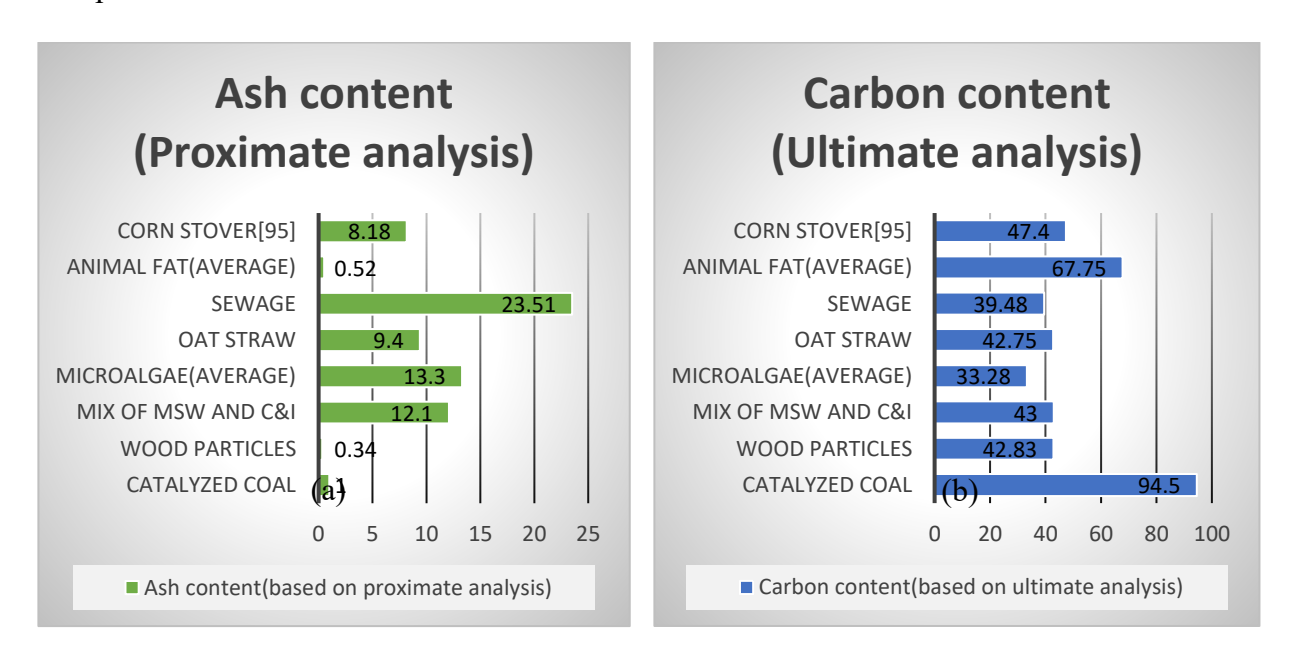


Figure 2.5: Carbon content of various types of biomass: (a) Ash content based on proximate analysis and (b) Carbon content based on the ultimate analysis [11,51-56]

2. 4. Optimization of Biomass Gasification Process

Table 2.2 is used to summarize some of the commercial biomass gasifiers based on their size and presents their performance by calculating CGE and carbon conversion [51]. As mentioned earlier in Section 2.3.3., the CGE is a demonstration of the amount of the chemical energy received by the syngas from the total chemical energy of the biomass. Table 2.2 shows one of the main drawbacks in the commercialization of the gasification plants which is the low value of CGE. According to Svishchev et al. [58], simulations have proven that a CGE of up to 124% can be achieved using an external heat, that is less observed in the existing plants. Svishchev et al. [58] stated that demonstration and pilot plants have lower efficiency because of either non-optimal operational conditions or due to the inappropriate choice of gasification method.

 Table 2.2: Performance characteristics of commercial biomass gasifiers [51]

Size (MW) ¹	Scale	Gasifier type	Agent type	Feedstock	Moisture wb% ²	Ash db%³	CGE %	Carbon conv.
26.5	Commercial	Shaft- furnace	Oxygen- rich air	Municipal solid waste	44	16.3	49.2	95.3
18.9	Commercial	Shaft- furnace	Oxygen- rich air	Municipal solid waste	42.8	32.3	54.6	91.7
2	Pilot	Bubbling fluidized bed	Air/steam	Sewage sludge	3–8	39.5	70	n/a
1.2	Pilot	Two-stage downdraft	Air	Wood chips	12.3	0.6	53	74
1.1	Demonstration	Updraft	Air, Air/steam	Municipal solid waste	30	11.7	32– 58b	n/a
0.5	Demonstration	Bubbling fluidized bed	Air	Sewage sludge	3–8	57	66	n/a
0.4	Pilot	Entrained- flow (cyclone)	Air	Peat, rice husk, bark, wood	<15	0.6– 19.3	43– 52	70–95
0.3	Pilot	Entrained- flow	O_2/N_2	Wood powder	3	0.9	58	89
0.25	Pilot	Downdraft	Air	Wood sawdust, pellets	9.5	2.1	68	n/a
0.06-0.08	Pilot	Bubbling fluidized bed	Air	Wood pellets	6.3	0.7	55– 60	89–95
0.04-0.07	Pilot	Bubbling fluidized bed	Air	Olive oil waste (orujillo)	8.7	14.2	53– 60	70–94

¹Megawatt / ²wet basis / ³dry basis / ⁴carbon conversion

2. 4. 1. Integrated gasification combined cycle

Although the conversion of solid biomass to syngas is the core of the gasification process, the sustainability of the process needs to be validated from a more comprehensive viewpoint. The concept of integrated gasification combined cycle (IGCC) has been recently introduced as a sustainable approach in designing biopower plants assisted with biomass gasification process. IGCC is a solution for making the sustainable conversion of biomass, from cradle-to-grave, through gasification technology. IGCC considers post-treatment of produced syngas to ensure the versatility of the process to be employed for a variety of applications such as heat, power, chemicals, liquid fuels and hydrogen fuel production. Hence, we discuss the post-processing of syngas in this section.

2. 4. 1. 2. Production of synthesis gas and chemicals from biomass

I- Syngas

Syngas is mainly a mixture of H₂ and CO plus CO₂ and CH₄. It is fuel as well as a feedstock for chemical and energy processes. Processing of fossil fuels is originally used to produce syngas. Biomass has been considered as a promising alternative source for producing the syngas, sometimes called as bio-syngas. One of the most prominent sectors in processing the syngas is South African Synthetic Oil Limited (SASOL) which has been producing liquid fuel from the syngas using Fischer-Tropsch synthesis (FTS). Depending on the processing method, syngas can be used to create a wide range of products such as (1) Hydrogen fuel in (bio)refineries, (2) Diesel or gasoline using FTS, (3) Methanol for the chemical industry, and (4) Fertilizers by processing ammonia. As mentioned earlier, the old method of reforming natural gasses using two catalytic paths produced syngas:

•
$$CH_4 + H_2O \rightarrow CO + H_2$$
 (Steam reforming of methane) (2.27a)

•
$$CH_4 + 0.5 O_2 \rightarrow CO + 2H_2$$
 (Partial oxidation of natural gas) (2.27b)

The desired hydrogen to carbon monoxide ratio (H₂/CO) determines the catalytic reactions. Every product demands a certain value of H₂/CO. For instance, if the goal is to produce gasoline, the ratio should be between 0.5-1 molecule of H₂ for one molecule of CO. This value for producing methanol changes to 2 roughly.

Low-temperature gasification can either produce the syngas from gasification (<1000°C) or high-temperature gasification (>1200°C). For the former case, the heavy hydrocarbons are formed which need to be further cracked to obtain the syngas. For the latter case, the products are mainly H₂ and CO. To adjust the H₂/CO, a well-known reaction, so-called as shift reaction is typically employed to achieve the desired ratio:

•
$$CO + H_2O \rightarrow CO_2 + H_2$$
 (2.28)

The syngas product must be cleaned-up prior to synthesized reaction, removing dust particulates and other rate-limiting gases. A general syngas treatment is water quenching to remove ash and char particles.

II- Bio-oil production

Bio-oil is any liquid derived from a living organism (e.g., plants). It is the liquid fraction of the biomass pyrolysis/gasification. Bio-oil is a dark-brown organic liquid, highly oxygenated which contains a significant amount of water (~25% volume). Its composition varies with the biomass type and the selected thermochemical process. Contrary to mineral oils, the properties of bio-oil may change with time; for instance, its viscosity increases, and its volatility decreases with time. Fast pyrolysis can also produce bio-oil, the result of which is called bio-crude. Bio-oil has several applications, for example as:

- (1) A substitution with furnace oil for energy production
- (2) A feedstock to produce chemicals such as resins, adhesives, and acetic acids
- (3) Liquid fuel for the transportation sector

III- Conversion of Syngas into Chemicals

III-A Methanol production

Methanol is an important raw material to produce many chemicals and fuels, such as gasoline. The synthesis of syngas (CO and H₂) in the presence of catalysts (Eq. 2.29) produce methanol, where the syngas is compressed before feeding into a fluidized-bed reactor for synthesis with a catalyst. The fluidized-bed reactor has the advantage of continuous catalyst regeneration and efficient removal of the generated heat, which is further cooled to form the condensed methanol:

$$n(CO) + 2H_2 \rightarrow CH_3OH \tag{2.29}$$

The Fischer-Tropsch synthesis in the next section explains definition "n" in Eq. (2.29).

III-B Fischer-Tropsch Synthesis

The Fischer-Tropsch process (FTS) is a group of reactions that converts syngas into liquid hydrocarbons. The process is of interest specifically due to the possibility of conversion of coal or biomass into synthetic fuels using this process. Among the series of reactions, Henrici-Olive et al. [59] presented the generic form of hydrocarbon production:

•
$$n(CO) + 2n(H_2) \rightarrow (CH_2)_n + n(H_2O)$$
 (2.30)

The (CH₂)_n molecules are called olefins, and n ranges between 5 and 10 for synthetic fuels. FTS process has been popular in industrial applications including but not limited to:

- (1) SASOL in South Africa which has been using coal to produce diesel fuel since 1952
- (2) Pearl GTL in Qatar which converts natural gas to petroleum liquid at a rate of 140000 barrels a day
- (3) Shell facility in Malaysia transforms natural gas into low-sulfur diesel fuels and food-grade wax (12000 barrels a day)

IV- Transport fuel from biomass

Biodiesel, ethanol, and biogas are transport fuels produced from biomass which can be potentially used in automotive, airplane, and locomotive. The application of these fuels is still being evaluated for considering as stand-alone fuels in the transportation sector.

IV-A Gasoline production from methanol

One of the processes to convert methanol to gasoline is called Exxon Mobil's MTG process, which results in C₅-C₁₂ hydrocarbons. The reaction is carried out in two dehydration stages: a first stage is to produce dimethyl ether intermediate and the second stage is to produce gasoline. The reaction can be written as [60]:

$$2CH_3OH \rightarrow (-H_2O) \rightarrow CH_3OCH_3 \rightarrow -H_2O \rightarrow C_2 -C_5 \rightarrow$$

Paraffins + Aromatics + Cycloparaffins
where (-H₂O) represents the dehydration steps. (2.31)

IV-B Biodiesel production

Biodiesel is generally produced from vegetable oil or animal fats with significant constituents that are triglycerides. Biodiesels are safer than regular types of diesel from the storage point of view due to a higher flash point of animal fats and plant oils compared to petroleum crude oil [61]. Furthermore, biodiesels can be used as lubricants which gives the engine a longer life. The high oxygen content of biodiesel assists complete combustion in an engine.

A popular production method involves mixing waste vegetable oil or fat with a catalyst and methanol (or ethanol) in appropriate proportion (typically 87% oil, 1% NaOH catalyst, and 12% alcohol). Since NaOH is not recyclable, research is being carried out to find a greener catalyst. For example, supercritical methanol (above 293° C, 8.1 MPa) can be used for the process, and it does not involve a catalyst [62].

IV-C Transport fuel from non-food biomass

Despite the capability of cereals for producing gasoline or ethanol, it has negative impacts on the food market due to causing a shortage of this feedstock. Therefore, an alternative solution is to employ cellulosic materials which can produce gasoline or ethanol by either a thermal or biochemical process [63]. In the thermal process, the cellulosic feedstock is subjected to fast pyrolysis, and the produced liquid fuel is refined into gasoline. The FTS process is a thermal route to convert cellulosic materials to gasoline. In the biochemical process, the steps leading to the production of cellulosic ethanol include mechanical cleaning, hydrolysis (conversion into sugar), fermentation (conversion of sugar into ethanol), distillation (removal of water and solids) and dehydration (final drying).

2. 5. Theoretical Modeling

2. 5. 1. Chemical equilibrium models

Thermo-chemical equilibrium modeling provides approximate predictions of syngas composition, which is independent of the gasifier geometry [64]. By assuming equilibrium, the maximum yield can be calculated based on the gasification of a particular biomass to evaluate process parameters suitable for the feasibility test of thermo-chemical conversion of alternative types of biomass [65]. The optimal conditions, e.g., energy efficiency and syngas heating value, can be predicted by this type of modeling for the operation of each specific reactor or power plant.

Shayan et al. [66] used a thermodynamic equilibrium model to simulate the biomass gasification process and conducted a parametric experimental study to validate the results of their model. They concluded that the highest energy and exergy efficiencies are achieved when air and steam were used as gasification medium, respectively.

2. 5. 1. 1. Constitutive equations

The chemical equilibrium uses two main methods: (i) Equilibrium constants or stoichiometric method and (ii) Minimization of Gibbs free energy or non-stoichiometric method. The main difference between these two methods is that the method of equilibrium constant requires the knowledge of each chemical reactions and reactants. However, the latter approach depends on the minimization of Gibbs free energy. Looking closely at previous studies shows that calculations for the stoichiometric method are far less complicated compared to the non-stoichiometric method [67]. It is noteworthy that both approaches are based on the same concept [33]; therefore, we acknowledge both methods as one in this study. In Table 2.3, the calculation procedure for chemical equilibrium modeling has been summarized [20, 45].

The typical global gasification equation among most models is [33]:

$$CH_{x}O_{y}N_{z} + wH_{2}O + m(O_{2} + 3.76N_{2})$$

$$= n_{H_{2}}H_{2} + n_{CO}CO + n_{CO_{2}}CO_{2} + n_{H_{2}O}H_{2}O + n_{CH_{4}}CH_{4} + (\frac{z}{2} + 3.76m)N_{2}$$
(2.32)

where x, y, and z are the number of atoms of hydrogen, oxygen, and nitrogen per number of atoms of carbon in the feedstock, respectively; w is the amount of moisture per kmol of feedstock and m is the amount of oxygen per kmol of feedstock. It is possible to take sulfur into account for the biomass components. For some certain biomass, there is a significant amount of sulfur to be considered. The procedure for calculations of syngas component and HHV for other equilibrium models is given in Table 2.3. However, the main difference between the various models is the way the authors determine the required assumptions.

Table 2.3: Equilibrium models for thermodynamic modeling.

Equilibrium constants [33]:

1. Mass balance for carbon, hydrogen, and oxygen:

$$\sum_{i} mass_{products} = \sum_{i} mass_{reactants}$$

$$\sum_{j} mass_{products} = \sum_{j} mass_{reactants}$$
 Considering global reaction in:
$$C: f_1 = 0 = n_{CO} + n_{CO_2} + n_{CH_4} - 1$$

$$H: f_2 = 0 = 2n_{H_2} + 2n_{H_2O} + 4n_{CH_4} - x - 2w$$

$$0: f_3 = 0 = n_{CO} + 2n_{CO_2} + n_{H2O} - w - 2m - y$$

2. Equilibrium constants for water-gas shift and methane reaction:

$$K_i = \prod_i (x_i)^{\mathcal{V}_i} (\frac{P}{P^{\circ}})^{\sum_i \mathcal{V}_i}$$

 $K_i = \prod_i (x_i)^{\nu_i} (\frac{P}{P^\circ}) \Sigma_i v_i$ x_i is mole fraction of species i in the ideal gas mixture, ν is the stoichiometric number (positive value for products and the negative value for reactants), Pois standard pressure, 1 atm, and n_{total} is the total mole of syngas:

$$\begin{split} K_1 &= \frac{(n_{CO_2})(n_{H_2})}{(n_{CO})(n_{H_2O})} \qquad K_2 = \frac{(n_{CH_4})(n_{total})}{(n_{H_2})^2} \\ 1. \qquad \text{Calculation of K using standard Gibbs function of reaction:} \end{split}$$

$$\ln K = -\frac{\Delta G_T^{\circ}}{\bar{R}T}$$

$$\Delta G_T^{\circ} = \sum_i \mathcal{V}_i \Delta \bar{g}_{f,T,i}^{\circ}$$

Where \bar{R} is the universal gas constant, 8.314 kJ/(kmol·K), ΔG_T^o is the standard Gibbs function of reaction, and $\Delta \bar{g}_{f,T,i}^{\circ}$ represents the standard Gibbs function of formation at given temperature T of the gas species i:

$$\Delta \bar{g}_{f,T,i}^{\circ} = \bar{h}_{f}^{\circ} - a'Tln(T) - b'T^{2} - \left(\frac{c'}{2}\right)T^{3} - \left(\frac{d'}{3}\right)T^{4} + \left(\frac{e'}{2T}\right) + f' + g'T$$

a'-g' and the enthalpy of formation of the gases can be found in [33].

3. Calculating temperature of gasification zone with energy balance with the assumption of adiabatic process and $T_{inlet} = 298K$

$$\sum_{i=react} \bar{h}_{f,j}^{\circ} = \sum_{i=read} n_i (\bar{h}_{f,j}^{\circ} + \Delta \bar{h}_{T,i}^{\circ})$$

 $\sum\nolimits_{j=react}\bar{h}_{f,j}^\circ=\sum\nolimits_{i=prod}n_i(\bar{h}_{f,j}^\circ+\Delta\bar{h}_{T,i}^\circ)\\ \bar{h}_f^\circ\text{is the enthalpy of formation in kJ/kmol, and }\Delta\bar{h}_T^\circ\text{represents the enthalpy difference between}$

$$\Delta \bar{h}_T = \int_{298}^T \bar{C}_p(T) dT$$

4. Calculating specific heat (assumption of constant pressure) in kJ/kmolK

$$\bar{C}_n(T) = a + bT + cT^2 + dT^3$$

$$\int_{298}^{T} \bar{C}_{p}(T)dT = aT + bT^{2} + cT^{3} + dT^{4} + \kappa$$

a, b, c, and d are the specific gas species coefficients and can be found in the literature.

5. Rewrite equations in part 4 with part 5 and using the following for finding the enthalpy of formation for solid fuel in reactant:

$$h_{f,fuel}^{\circ} = \overline{LHV} + \sum\nolimits_{k=prod} [n_k {\left(\bar{h}_f^{\circ} \right)}_k]$$

Minimization of Gibbs free energy with Lagrange multiplier method [68]

1. The total Gibbs energy of the system at specific Temperature

$$G_{T,P}^t = g(n_1, n_2, n_3, ..., n_i)$$

 n_i is referred to each species in the system.

We want to find the set of n_i that minimizes the total Gibbs energy:

2. Material balance:

$$\sum_{i} n_{i} a_{ik} = A_{k} \ (k = 1, 2, \dots, w)$$

 a_{ik} is the number of atoms of the k^{th} element present in each molecule of the chemicals species I, A_k is the total number of atomic masses of the k^{th} element in the system and w is the total number of atoms present in the system.

3. Introducing Lagrange multipliers:

$$\sum_k \lambda_k (\sum_i n_i a_{ik} - A_k) = 0$$

4.Defining a new function:

$$F = G_{T,P}^t + \sum_k \lambda_k (\sum_i n_i a_{ik} - A_k)$$

5. Deriving minimum value of F:

$$\frac{\partial F}{\partial n_i} = \frac{\partial G^{\tau}}{\partial n_i} + \sum_k \lambda_k a_{ik} = 0 \; , \qquad (i=1,2,\dots,n) \label{eq:final_final}$$

6. Replacing chemical potential in Eq. (5):

$$\mu_i + \sum_k \lambda_k a_{ik} = 0$$

7. Definition of chemical potential:

$$\mu_i = G_i^0 + RT ln(\frac{f_i}{f_i^\circ})$$

where G_i^0 is the standard state Gibbs energy of formation, R is the universal gas constant, T is the temperature and f is the fugacity of

In case of ideal gas assumption at standard pressure and using Eq. (7) in Eq. (6) we have:

$$G_i^0 + RTln(\frac{n_i}{n_{total}}) + \sum_k \lambda_k a_{ik} = 0$$

$$(i = 1, 2, ..., n)$$

Therefore, we have n equilibrium equations for each species present in the system.

The mass balance for each element and energy balance is written like equilibrium constants to be solved for HHV.

A summary of some commonly used assumptions is mentioned in the following [40]:

- (1) Carbon, hydrogen, oxygen, and nitrogen are the only elements considered forming biomass
- (2) The system has uniform pressure and temperature and is found in the steady state
- (3) The system reaches equilibrium state which is a result of a specific range for reaction rate and residence time
- (4) Syngas components (H₂, CO, CO₂, CH₄, H₂O, and N₂) are considered as ideal gases
- (5) The total amount of tar is used in the reaction zone
- (6) If any char leaves the reaction zone, it will remain unreacted

Without modification, results show a significant deviation between theoretical models and experimental calculations of syngas components. This gap is mainly due to the idealistic equilibrium assumption in cases that residence time is not long enough. Another unrealistic assumption is neglecting the existence of tar and residue. In addition, there is a limitation for the temperature range when reaching equilibrium and it can be as high as 1500K. According to Altafini et al. [69], for a higher temperature than 1073K, stronger tendency to CO and H₂ formation compare to CO₂ and H₂O exists, which is a result of temperature-dependency of standard Gibbs free energy. For temperature values lower than 673K, which falls into a pyrolysis region, the formation of CH₄ affects the output. Both outputs create a gap between the experimental results and equilibrium model predictions.

Applying empirical constants for modification of equilibrium constants are used to consider the effect of incomplete carbon conversion and heat loss. Joel et al. [40] reported that carbon conversion is generally between 85 to 95% depending on the type of gasification process and shows an ascending behavior as the temperature of reactor goes up until it reaches a maximum value. From the maximum point, we observe a constant carbon conversion, which could be defined based on equilibrium ratio and temperature [70]. These quasi-equilibrium equations use constants that are mainly based on limited experiments without a robust theoretical justification leading to a considerable error for specific syngas components such as H₂ and CH₄.

In a nutshell, equilibrium modeling is still a useful method as a preliminary step for designing a gasifier, especially for downdraft gasifiers since oxidation zone (the hottest zone in the system) is

the area that pyrolysis and gasification products are forced through resulting in a closer situation to the equilibrium condition for the faster rate of reaction [10]. In this article, the focus is on novel methods resulting in much higher accuracy for thermochemical equilibrium models. Reviews of thermochemical models of gasification have been broadly discussed in the literature [67, 71].

2. 5. 1. 2. Plasma technology

The plasma technology has recently received attention as an external energy source using ionized plasma gas to help systems to reach steady state. The primary application for the plasma systems is thermal waste treatment [72]. In this application, plasma technology helps in achieving a complete decompose of the waste and replacing the tar in the syngas by the slag which is environmentally friendly and stable. In addition, great potential for plasma gasification has been applied for the production of syngas from biomass. The main advantages of this system according to Materazzi et al. [11] are low residual levels of tar and sulfur as well as possessing a stable heat independent on the chemistry of the reactions [73]. Materazzi et al. reported the disadvantages of one stage plasma gasification as required oxidant addition, power input and emission control depending on unstable residues such as char and tar. The amount of residues depends on either the biomass feedstock or the operational parameters [74]. Cortazar et al. [75] reported the direct relationship between temperature and tar removal during the gasification of sawdust. The tar removal was ascribed to its evolution to make aromatic compounds at higher temperatures more stable.

Two-stage plasma technology has been introduced to overcome these drawback. The two-stage system demonstrates two main steps in gasification: first being pyrolysis and the second one is the reduction zone. Each stage has separate heat and oxygen intake and char production. As a result of this configuration, the system has high carbon efficiency and high-quality syngas output (specifically a more considerable amount of CO and H₂) and low amount of tar residues. Using plasma technology favors the process by reducing oxygen needed in the second stage compared to non-plasma two-stage gasification systems.

Consequently, two-stage plasma technology is a desirable process for energy production from waste gasification. However, it is worth mentioning that plasma technology has high electrical consumption resulting in high investment costs to reduce efficiency as compared to conventional methods [76]. A summary of existing plasma generators is presented in Table 2.4 [77].

 Table 2.4: Plasma torches for plasma chemical technologies [77].

Institution	Work g	gas	Power	Application
			(kW)	
Persee-Mines	СхНу		Up to	Carbon nanotubes synthesis
Paristech, France			20	and waste treatment
University of Toronto, Canada	CO ₂ /C	H4	70	Plasma spraying, waste treatment
Westinghouse Plasma Corp., USA	Air, O ₂	2	5– 2400	Waste treatment
Phoenix Solutions Company, USA	Air, CO ₂ , C	O ₂ ,	10– 3000	Waste treatment
Europlasma group, France	Air,	CO ₂ ,	100-	Waste treatment, gas
	CO		4000	purification, immobilization of radioactive waste
Pyrogenesis, Canada	Air,	O ₂ ,	50-	Waste treatment,
	CO ₂ , H ₂ O	CO,	1000	destruction of refrigerants, gasification
Seoul National University, Korea	Air		40– 300	_
Research Institute of Experimental and Theoretical Physics of Al-Farabi Kazakh National University, Kazakhstan	Air		50– 200	Coal combustion
Khristianovich Institute of Theoretical and Applied Mechanics SB RAS, Russia	H ₂ O		10– 150	_
A.V. Luikov Heat and Mass Transfer Institute of the National Academy of Sciences of Belarus, Republic of Belarus	H ₂ O		50–75	Toxic ash processing
Lithuanian energy institute, The Republic of Lithuania	H ₂ O		25–45	Waste and biomass treatment
-	H ₂ O		8–32	Plasma spraying, destruction of halocarbon
Kyungsan University, South Korea	H ₂ O		50– 200	Toxic waste treatment
Paton Electric Welding Institute of NAS of Ukraine, Ukraine	H ₂ O		160	Waste treatment
Lonza Ltd, Switzerland	H_2O		250	TiO2, TiC synthesis
Institute of Plasma Physics, Czech			80–	Biomass and waste
Republic			200	gasification

In addition, Table 2.5 summarizes some of the recent experimental studies with plasma torches based on the biomass type. Type of plasma gas and method of production of plasma can be found alongside the type of biomass.

Table 2.5: Plasma Torches and different types of biomass.

	[77]	[78]	[79]	[80]	[73]	[81]	[82]
Plasma gas	Air	Air	Nitrogen	A mixture of Ar and H2O	Not mentioned	argon, nitrogen, and air	Nitrogen
Method of production	Alternating current (AC)	Alternating current (AC)	Microwave	Hybrid stabilization/ DC electric arc	Direct current (DC)	Alternating current (AC)	Direct current (DC)
Type of biomass/ biofuel	Coal, wood, and RDF	Wood residues	Glycerol (a byproduct of biodiesel production)	Spruce sawdust, wood pellets	Refuse- derived fuel (RDF)	Corn cob	High-density polyethylene

2. 5. 2. Kinetics

Equilibrium modeling does not provide sufficient information on how to design a gasifier. Kinetics modeling is used to combine operational parameters of a gasifier, e.g., residence time, length of reactor and reactor hydrodynamics. In a rate dependent model, a detailed reaction mechanism with the rate of each reaction is considered depending on the type of fuel used. The main difference between equilibrium constants modeling and kinetic modeling is that in the latter all the possible reactions is considered whereas only specific reactions are selected in equilibrium constants modeling. Therefore, the process for kinetics modeling is computationally intensive and somewhat complicated.

To simplify the process of modeling and to write the reactions, we break down the whole process into three phases as pyrolysis, oxidation, and reduction. These three phases are the basis for developing the gasification models. As for pyrolysis, three different types of model exist (1) one-step reaction, (2) two-step reaction, and (3) three-step (or more) reaction. Due to the complexity of more than two-step reaction, it is assumed that no more than two steps for each reaction exist.

Parameters for any equation used to rely on the individual experiments leading to significant variation in the values reported in the literature. The output of rate-based modeling of pyrolysis is the amount of volatile used in the gasification part and includes the oxidation and reduction. However, the yield of the main components of syngas will not be calculated for this type of modeling.

Pyrolysis can be described by three simplified main kinetics schemes similar to Figure 2.6 [83].

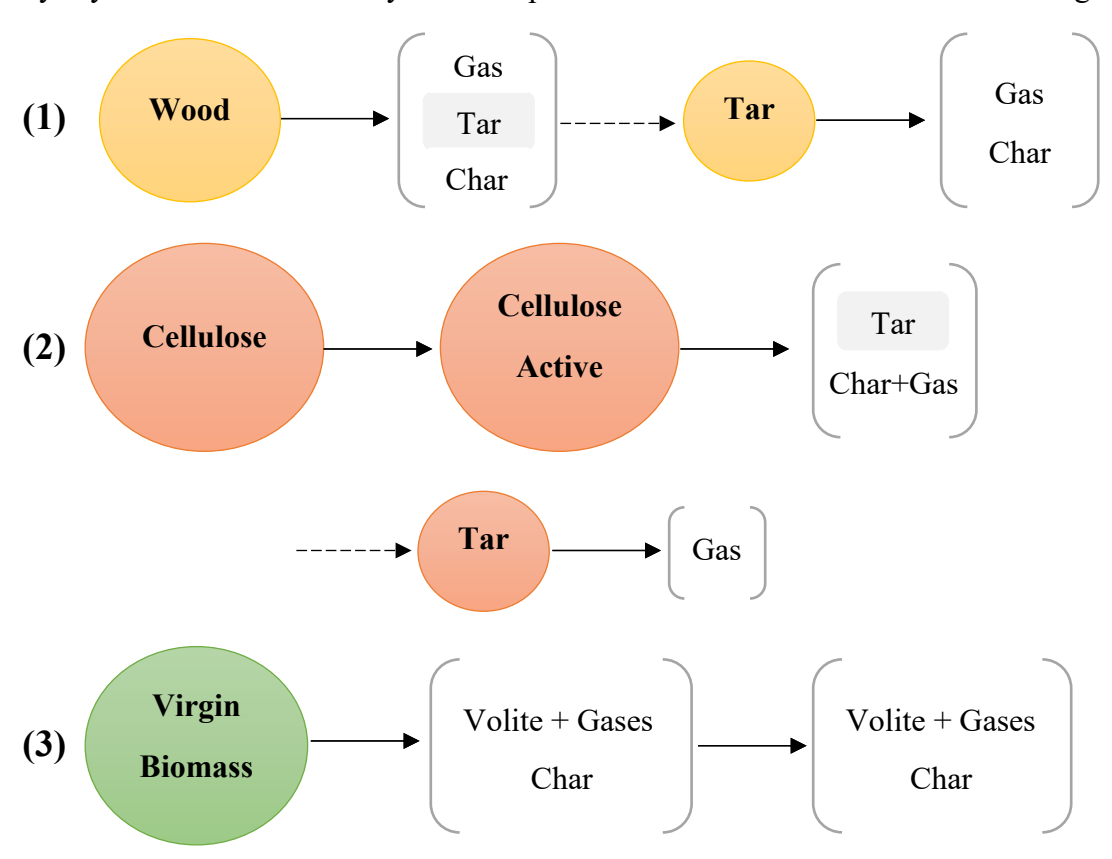


Figure 2.6.: Main kinetics schemes for wood gasification

As Babu et al. [83] mentioned scheme 3 is an ideal option since scheme 1 lacks accuracy due to the assumption of the constant ratio between the yields of solid char and gaseous products. Scheme 2 also requires kinetics data for the intermediate active state of biomass which is not usually reported in the literature. Based on scheme 3, a simplified model for gasification can be introduced using Table 2.6 [15].

Table 2.6.: Summary of fundamental reactions in the gasification process of biomass. [15]

Chemical reactions
$C < S > +0.5O_2 = CO$
$C < S > + CO_2 = 2CO$
$C < S > + H_2O = CO + H_2$
$CO + 0.5O_2 = CO_2$
$H_2 + 0.5O_2 = H_2O$
$CO + H_2O = CO_2 + H_2$
$CO_2 + H_2 = CO + H_2O$
$CH_4 + O_2 = CO_2 + 2H_2O$
$CH_4 + H_2O = CO + 3H_2$
$CO + 3H_2 = CH_4 + H_2O$

Copyright has been granted by the publisher

Char reactivity factor (CRF) has recently received attention since it is one of the main parameters affecting the kinetics of the gasification process. The rate of this factor determines the amount of syngas produced in the next steps. There are different alternatives to models describing the physical changes occurred in biomass as a result of char production. As Lopez et al. [84] mentioned, there are three primary models considering physical changes of biomass: (1) Homogenous model (2) Shrinking core model (SCM)and (3) Random pore model (RPM). Knowing the range of reaction temperature helps to choose one of these models. Since temperature controls the mass transfer limitations, the temperature can be used as a source to determine the state of char reactions.

Temperature changes can be determined according to an Arrhenius plot similar to Fig.2.7 which is a logarithmic plot of reactivity versus inversed temperature [85], and the slope of curve presents the activation energy of the reaction. This plot can be divided into three main regimes: In regime I, reactions take place on the surface of char in a somewhat uniform state while chemical reaction controls the gasification. In regime II, reactions extend from the surface of the char to its inner part, and it is controlled by pore diffusion rate rather than chemical reaction itself. For the last

Controlling reaction for each regime

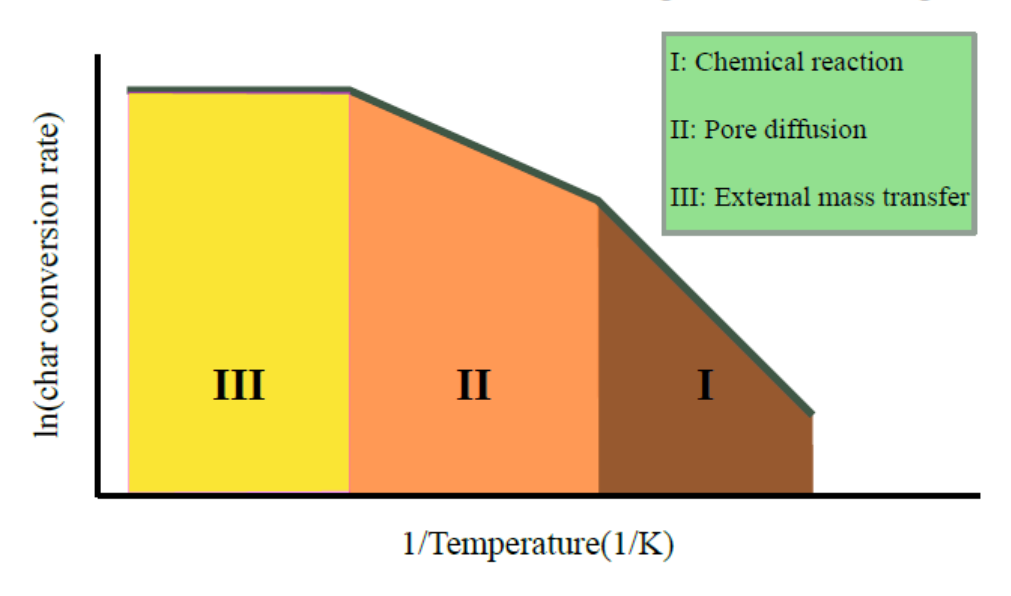


Figure 2.7: Logarithmic plot for reactivity versus inversed temperature for char conversion

regime, a diffusion process is formed from the surface of the char to bulk phase eliminating the effect of the temperature on the gas concentration. For the homogeneous model, the reaction propagating throughout the volume of the char is assumed to occur homogeneously with a constant reactivity. One of the proposed modifications for this model is to add the reaction order or "n" as the power of reaction rate; this value is evaluated empirically [86].

As for the SCM model, the change of volume is considered, and the homogenous reaction is assumed to take place only on the surface of a spherical model, as the core of the biomass remains unreacted. The size of the core is a function of char conversion rate. The scanning electron microscopy (SEM) of char, carried out by Adeyemi et al. [87], indicated the porosity of three stages for the formation and evolving of pores. Three different groups of char residues have been classified based on char's porosity, and structure [88], where the group I has the highest porosity and thinnest wall formation and group III has the thickest wall and low porosity accordingly. Adeyemi et al. observed that as a first step, group III chars are created through micro-pores around very active sites; with the reported porosity of lower than 40%. Then, group II and I char particles are developed by possesses meso-pores and macro-pores, with the porosity of char having more than 20% growth. Finally, the walls become fragile, and the char is fragmented and converted into ash.

An example of using SCM can be found in reference [89], where SCM has been used to simulate char gasification in fluidized bed gasifier. The following figure illustrates these steps based on the

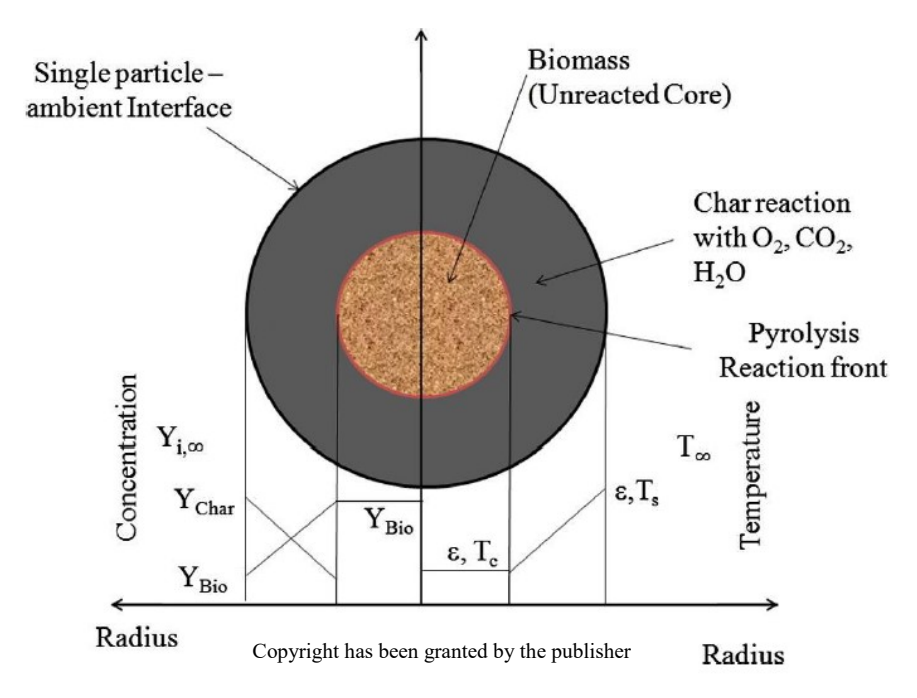


Figure 2.8: Schematic diagram of the processes for Gasification occurring at the particle level [90].

radius of the biomass indicating the change in concentration and temperature within the element [90]:

PRM modeling considers specific active sites by observing changes leading to pore growth and coalescence. In this type of modeling, pores are considered cylindrical, and the reaction is happening on the surface of this pores that do not overlap with each other. The kinetics equations of these models are summarized in Table 2.7 [84]:

Table 2.7: Rate of char gasification based on their kinetics model [84]

Model	The rate of Char gasification
Homogenous model	$\frac{dX}{dt} = kP_{H_2O}^{\alpha}(1 - X) $ (33)
SCM	$\frac{dX}{dt} = kP_{H_20}^{\alpha} (1 - X)^{\frac{2}{3}} $ (34)
RPM	$\frac{dX}{dt} = k \frac{S_0}{1 - \varepsilon_0} P_{H_2O}^{\alpha} (1 - X) [1 - \psi \ln(1 - X)]^{1/2}$
	(35)

where X is the conversion Rate of char which can be defined as the ratio of the mole number of the products at a particular time to the total amount of products in the complete conversion. In addition, ψ denotes the effect of the porous structure of char [84].

$$\psi = \frac{4\pi L_0 (1 - \varepsilon_0)}{{S_0}^2} \tag{2.36}$$

where S_{θ} ε_{θ} and L_{θ} denote surface area, total volume and length of the porous system made up of random overlapping pores.

Another factor determining the char model is the crystalline microstructure of char and biomass, affecting the particle homogeneity. It is worth mentioning that multiscale homogenization technique [91] is also a computationally efficient method for predicting useful properties of biomass.

Huo et al. [27] calculated carbon crystallinity of biomass char using the ratio of stacking heights to the spacing between graphitic sheets and demonstrated relation of crystallinity and gasification reactivity of the char. They concluded that increasing char crystallinity results in a lower gasification reactivity. It is worth mentioning that crystallinity changes during the gasification process, a phenomenon which has been studied by Zhou et al. [92].

As the next step toward modeling, submodels can be extracted to simplify the simulation of gasification. Tremel et al. [85] used a model based on pyrolysis, intrinsic reactivity, surface area, char deactivation, boundary layer diffusion, particle size, and pore diffusion submodels to precisely simulate the gasification process. The mentioned submodels commonly make coupling between kinetics and transport phenomena to improve the accuracy of modeling gasification [70, 71]. Ranzi et al. [93] considered solid and gas phase kinetics at both particle and reactor scales. Loha et al. [9] developed a three-dimensional kinetics model coupled with gas-solid hydrodynamics to demonstrate flow pattern and gas composition in bubbling fluidized bed gasification.

Overall kinetics modeling can be a useful approach to study gasification, especially for design and optimization of gasifiers. Reactor's hydrodynamics and residence time in gasifier systems are among the outputs of kinetic modeling [67]. However, kinetics modeling is more complicated than

thermodynamics and requires several assumptions which yet to be validated theoretically and measured experimentally. Coupling kinetics with transport phenomena provides a relatively extensive insight into the gasification process.

2. 5. 3. Computational fluid dynamics (CFD) modeling

The computational fluid dynamics (CFD) modeling is one of the most advanced and affordable tools for analysis of the gasification process in a reactor [94]. The CFD simulation of a system provides the temperature profiles of the furnace, solid and gas phases [95], as well as a complete coupled chemical and fluid mechanical analysis of the bed [96]. Though mainly used for a fluidized or entrained bed, CFD can also be used for optimization of fixed beds to study the gasification process characteristics such as operation parameters, kinetics and physical properties of the feedstock [97]. A reliable CFD model can be based on the exact geometry of the industrial scale gasifier, thus eliminating the issues accompanied by scaling down [94]. Fernando et al. [94] stated that due to the flexibility of the CFD model for the number of parameters that can be changed (particle size, superficial velocity, moisture content, etc.), size optimization is one of the main application of this type of modeling. The vast number of research available in the literature regarding the CFD modeling creates the platform to enhance the understanding of multiphase flow behavior in polydisperse gas-solid reactors [98].

The CFD modeling focuses on describing the transport phenomena in the fluid phases and considers possible mass and energy transport and chemical reactions [99]. The transport phenomena can be caused as a result of fluidization, which is described as the phenomenon of the movement of solid particles caused by either the force of gravity, impulsion of Archimedes or the drag force existing in the system [95]. Thus, a simple force balance verifies the minimum velocity that enables the gas phase to move the particle by circulating, called fluidization velocity. In the case of the fluidized bed, this circulation results in a turbulent flow, which is commonly described by the standard k– ε model that uses Navier-Stokes equations for velocities as the sum of mean flow and an instantaneous flow [95]; the model specifications can be found in reference [100].

In general, dynamic models are categorized in two main types: (1) macroscopic fluid dynamics models (MFD) and (2) CFD; whereas CFD modeling is preferred due to higher accuracy [101]. The CFD modeling of fluid dynamics of the biorefinery reactor has two main categories regarding gas-particle interactions: Eulerian-Lagrangian which includes discrete element model (DEM) as

well as discrete phase model (DPM), and Eulerian-Eulerian (two-fluid continuum) method [98]. The Eulerian-Lagrangian method only considers the fluid phase as a continuum, opposed to the Eulerian-Eulerian method which considers both fluid and particles as a continuum, thus called a two-fluid continuum. The Eulerian-Lagrangian category is recognized as the most accurate option for the particle motion, as well as for chemical reactions and heat and mass transfer on the particle scale, whereas the Eulerian-Eulerian approach lacks simplicity for describing mass, momentum and energy transfer [102] and is problematic where there are more than one type of particle [103]. However, the Eulerian-Lagrangian method is not economical for large-scale reactors compared to Eulerian-Eulerian, hence it is mainly used in particle-level studies [97]. In addition, a Eulerian-Lagrangian method is suitable for systems such as entrained bed gasifiers with particles in motion, and it is not a reliable method for packed bed; Eulerian-Eulerian is the most suitable for fluidized bed gasifiers [104]. A review of CFD models for biomass gasification can be found in reference [10].

2. 5. 4. Heat transfer

One of the most common approaches for modeling the gasification process is using heat and mass transfer concepts [3, 42, 92, 105-116]. Dasappa et al. [117] demonstrate as a great example of the concept behind these type of modeling. As a first step, the 1D particle is analyzed considering the changes with time for the concentration of products gas as well as reactants. The heat balance here is the sum of conduction within particle, heat produced during the reactions as well as radiation on the surface. Inconsistencies exist in the literature on claiming for a heat mode to have a higher value than the other, but overall convection is assumed to have a more significant impact compared to conduction. Radiation depends primarily on the temperature range of reaction, and therefore its influence and different radiation models are further discussed in [118].

The mass transfer uses kinetics to calculate gasification reactions rates used in energy balance equations. The greatest challenge at this stage is the change of parameters such as air properties, the density of char and gas, porosity and rate constants with temperature making it an unsteady case and dependable on specific assumptions such as average rate constants and constant air properties. Thus, it is nearly impossible to solve these equations without the help of numerical solutions such as finite element modeling (FEM). As the next step for this modeling, Dasappa et al. [44] used the temperature of the surface, and mass flux are results of 1D particle model to

model the whole bed with time. For the bed modeling, external heating (from heaters), as well as heat losses through convection, is added to the heat balance [119]. The latest version of this model has been used in reference [51] and summarized with the conservation equations in Table 2.8. Other modifications to Dasappa et al. [44] model have been made by considering two and threedimensional models, as well as the changes in all the parameters dependent on temperature and summarized in Table 2.9.

Table 2.8: Heat transfer modeling gasification process with conservation equations [51].

$$\frac{\partial(\rho\varepsilon)}{\partial t} = -\nabla \cdot (\rho V) + \dot{\varpi}_c''' \xrightarrow{Semi\ quasi\ equilibrium} \frac{\partial(\rho u)}{\partial x} = \dot{\varpi}_c''' \ or \ \frac{\partial(\dot{m}'')}{\partial x} = n\dot{m}_p$$
untion:

1. Species conservation equation:

$$\frac{\partial (\rho \epsilon_b Y_i^{\perp})}{\partial t} + \frac{\partial (\dot{m}^{"} Y_i)}{\partial x} = \frac{\partial}{\partial x} D \frac{\partial Y_i}{\partial x} + n [\dot{m}_p Y_{i,s} + K_D (Y_{i,s} - Y_i)] + \dot{\varpi}_c^{""}$$

the equation for mass conservation of i^{th} pellet: $\frac{\partial (\rho \epsilon_b Y_l)}{\partial t} + \frac{\partial (\dot{m}^t Y_l)}{\partial x} = \frac{\partial}{\partial x} D \frac{\partial Y_l}{\partial x} + n [\dot{m}_p Y_{l,s} + K_D (Y_{l,s} - Y_l)] + \dot{\varpi}_c^m$ Y_l is the mass fraction of i^{th} species and $Y_{l,s}$ is Y_l at the surface, $\rho(kg/m^3)$ is density, $m''(kg/m^2.s)$ superficial mass flux passing through the bed, n is the number of particles per unit volume, ϵ_b is bed porosity, D (m^2/s) is Diffusivity, $K_D(kg/s)$ is the mass transfer coefficient for the gas film surrounding the particle and $\dot{\varpi}_c^{\prime\prime\prime}$ (kg/m³. s) is volumetric char reaction rate term.

2. Gas phase energy conservation equation:

$$\frac{\partial (\rho \epsilon_b C_P T)}{\partial t} + \frac{\partial (\dot{m}^{"} C_P T)}{\partial x} = \frac{\partial}{\partial x} \kappa \frac{\partial T}{\partial x} + H_R + n \left[\dot{m}_P C_P T_{gas} + h A_s (T_{gas} - T) \right] + h_l A_{sr} \Delta T$$

T (K) is temperature, $C_P(kJ/kg.K)$ is specific heat, κ (W/m.K) is porous char's thermal conductivity, $H_R(J)$ is net radiation absorbed, $m_P(\text{kg/s})$ Gasification rate of one particle, $A_s(\text{m}^2)$ is the surface area, $h(W/\text{m}^2.K)$ is the heat loss coefficient and h_l is Reactor heat loss coefficient.

3. Radiation: It has been assumed that all particles have a uniform surface temperature and this temperature is calculated based on the average height of particles in the bed. The total radiative flux on the surface is:

$$Q = \sum_{j} f_{j} \sigma T_{j}^{4}$$

f stands for view factor. The net radiation absorbed by one particle is Q deducted from the radiation leaving the particle. Radiative

$$H_R'' = A_s \alpha (Q - \sigma T_s^4)$$

For modeling a single particle, the following equations apply:

For transient, spherical and one-dimensional analysis, we have the following conservation equations:

$$\frac{\partial}{\partial t}(\rho\epsilon) = \frac{1}{r^2} \frac{\partial}{\partial r} (-\rho v r^2) + \dot{\overline{w}}_c'''$$
2. Species conservation:

$$\frac{\partial}{\partial t}(\rho \epsilon Y_i) = \frac{1}{r^2} \frac{\partial}{\partial r} \left(-\rho v r^2 Y_i + r^2 \rho D_e \frac{\partial Y_i}{\partial r} \right) + \dot{\varpi}_c^{m}$$

Energy conservation equation:
$$\frac{\partial}{\partial t} (\rho C_p T) = \frac{1}{r^2} \frac{\partial}{\partial r} \left(-\rho v r^2 C_p T + r^2 \kappa \frac{\partial T}{\partial r} \right) + \omega_c$$
Porosity

$$\frac{\partial \epsilon}{\partial t} = -\frac{\dot{\varpi}_c'''}{2}$$

 $\frac{\partial \epsilon}{\partial t} = -\frac{\dot{\varpi}_c'''}{\rho_c}$ For the quasi-steady gas phase, the species and energy conversion can be redefined as follow: Energy conversion: $\frac{\dot{m}C_P}{4\pi r^2}\frac{\partial T}{\partial r} = \frac{1}{r^2}\frac{\partial}{\partial r}(r^2\kappa\frac{\partial T}{\partial r})$

$$\frac{\dot{m}C_P}{4\pi r^2}\frac{\partial T}{\partial r} = \frac{1}{r^2}\frac{\partial}{\partial r}(r^2\kappa\frac{\partial T}{\partial r})$$

Species conservation:

$$\frac{\dot{m}}{\pi r^2} \frac{\partial Y_i}{\partial r} = \frac{1}{r^2} \frac{\partial}{\partial r} \left(r^2 D_e \rho \frac{\partial Y_i}{\partial r} \right)$$

 $\frac{m}{\pi r^2} \frac{\partial Y_i}{\partial r} = \frac{1}{r^2} \frac{\partial}{\partial r} \left(r^2 D_e \rho \frac{\partial Y_i}{\partial r} \right)$ Lewis number is equal to one. The last two equations are solved, and we then differentiate the solution at $r=r_s$ which is the at the surface of biomass

Table 2.9: Heat transfer modeling of gasification.

Article	[51]	[120]	[42]	[113]	[113]	[20]	[92]	[105]	[121]
Assumptions									
Bed type	Di	D	D	T^{ii}	T	E ⁱⁱⁱ	Piv	CF ^v	S ^{vi}
Dimension	1	1	2	3	0	1	1	3	3
Steady	×	×	✓	✓	✓	✓	×	✓	✓
Convection	✓	✓	✓	✓	×	✓	✓	✓	✓
Conduction	✓	×	✓	×	✓	✓	✓	×	✓
Radiation	✓	✓	✓	✓	✓	✓	✓	✓	✓
Diffusion	✓	✓	✓	✓	✓	✓	×	✓	×
Condensation/ Vaporization	×	✓	×	×	×	×	×	×	×
Particle Shrinkage	✓	×	✓	×	×	×	×	×	×
Particle porosity	✓	×	×	✓	✓	✓	✓	✓	×
Void fraction of bed	✓	✓	✓	✓	✓	*	✓	*	×

ⁱ Downdraft packed bed (Co-current), ⁱⁱ Thermogravimetric analyzer, ⁱⁱⁱ Entrained bed, ^{iv} Packed bed, ^vCirculating fluidized bed, and ^{vi} Multiple tubes solar reactor.

2. 6. Concluding remarks

The present work provides an in-depth guideline for developing an appropriate theoretical and computational model for the gasification process. Figure 2.9 summarizes the outputs that are expected from each model. The primary parameters and the existing connection between the expected outputs have been identified in this figure by an arrow. As an example, the temperature of the gasification zone or T_{gz} is the output of the equilibrium model which can be used as the first input of iterations for deriving temperature distribution in char. Considering the complexity of gasification and a vast number of parameters, accurate numerical models are yet to be developed.

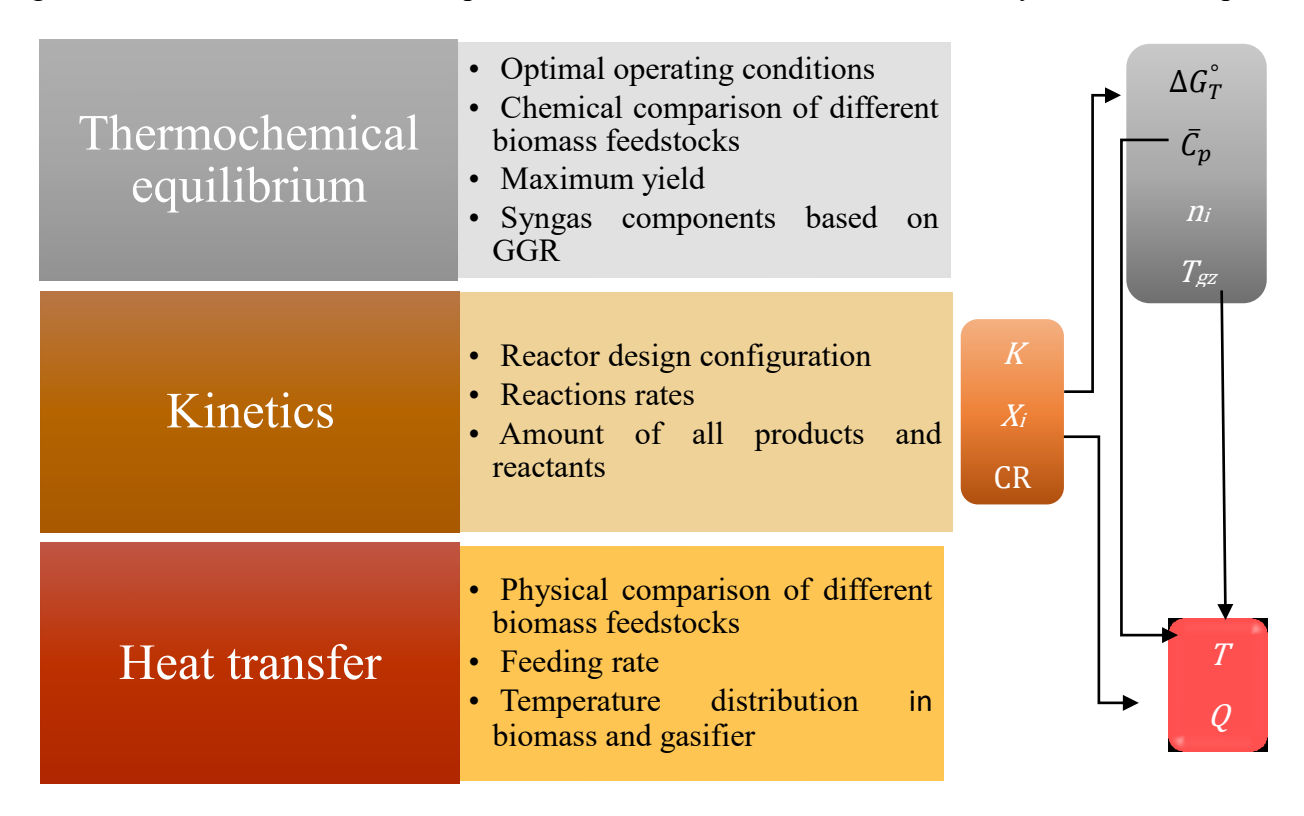


Figure 2.9: Summary of gasification models based on the output of each and the variables used

The current literature lacks a comprehensive strategy to model all types of gasifiers flexibly. Another major drawback of the existing gasification models is that they have focused specifically on syngas and reactions rather than the gasifiers for evaluating their energy efficiency. This review paper presents the main drawbacks of existing models of gasification along with a comprehensive review on gasification models to shed light on the pathways for improving the gasification process and to better evaluate the efficiency of advanced biofuels as an alternative sustainable energy resource.

Acknowledgments:

Authors acknowledge the financial support provided by BioFuelNet Canada and McGill University for conducting the research.

2. 7. Connecting statement

In the previous section, an extensive literature review on the gasification and its modeling process were conducted to clarify the basics of this phenomena and to help with the comprehension of the next chapters. Following chapter focuses on applying homogenization method to design numerical modeling of the cubic wood-plastic composites (WPC). This model can be beneficial for studying WPCs as a promising feedstock of the gasifiers in the near future.

CHAPTER 3: Numerical homogenization model of effective thermal conductivity for wood-plastic composites

Numerical homogenization model of effective thermal conductivity for woodplastic composites

N. Mazaheri, A.H. Akbarzadeh, A. Mirabolghasemi, M. Lefsrud

Department of Bioresource Engineering, McGill University, Ste-Anne-de Bellevue, QC H9X 3V9, Canada

Abstract

Wood plastic composites (WPCs) have gained attention in the last decades due to the possibility of designing their physical and thermal properties, as well as developing a cheap alternative for recycling wood and plastic wastes. Researchers have focused on experimenting and gaining knowledge on the effect of changing the matrix and inclusion materials, while fewer studies have been done for computational modeling of their behaviors. Effective thermal conductivity (ETC) of WPCs is one of the most critical thermal properties when used as biofuel in energy industries. In this article, a short review of the available analytical and computational models in the literature for calculating ETC of WPC is provided, and the effect of thermal conductivity of each phase on the overall ETC is studied. A 3D numerical homogenization model with cubic unit cells have been developed using finite element method (FEM) implemented in a commercial FEM software (ANSYS) to determine the effective thermal conductivity of porous wood-char with the different volume fraction of high density polyethylene (HDPE) fillers. Furthermore, the effect of the solid volume fraction in the composite and plastic content are studied.

3. 1. Introduction

The production of WPC or wood thermoplastic composites is predicted to grow more than half to meet the demand of different industries such as automotive and construction [122]. Primarily, WPCs were introduced as a new replacement for recycling methods of plastic and wood residues [123], thus reducing sustainability issues associated with those methods [124]. Later, as researchers experimented with the pyrolysis and the gasification of WPCs, other benefits of WPCs were discovered. Increasing the liquid biofuel production in pyrolysis of WPCs and enhancing hydrogen production in the gasification for the polyolefin polymers are among these benefits [125]. In addition, WPCs enlarge the energy density of the fuel compare to using wood biomass or plastic alone in different gasifiers [126, 127].

With the addition of the plastic to woody biomass, pyrolysis is altered to a two-step process. The decomposition of WPC starts with wood-fiber, which requires a lower temperature [128]. By increasing the temperature, the polymer is decomposed to hydrocarbons with a wide range of molecular weights as the next step. Therefore, a higher temperature leads to products with greater hydrocarbon content from plastics [125]. Pyrolysis of WPCs are mainly used to produce light liquid fuels with higher yield, and hydrogen content compare to woody biomass [126]. The main drawbacks of the pyrolysis process of WPC are the increase in methane, tar, and CO₂ production. However, Lopez et al. [129] observed that these issues are eliminated when the temperature is increased above 830 °C, and the gasification and Boudouard reactions start. They reported reformation of tar and methane that have been produced at lower temperatures and an overall enhanced tar and methane contents for the gasification with the addition of high density polyethylene (HDPE) plastic. Lopez et al. stated that the gasification process could be used to improve production of syngas hydrogen content, as well as the gas yield and carbon conversion efficiency.

While studying the gasification process of woody biomass, one of the principal parameters to consider is the effective thermal conductivity (ETC) [130-132]. Di Blasi et al. [130] concluded longer conversion time as the thermal conductivity decreases and thus results in better syngas quality. Suleiman et al. [131] experiments showed that a higher porosity of the wood biomass leads to inferior thermal conductivity and concluded conduction through voids of the structure of the wood is the primary parameter affecting overall heat conduction. Babu et al. [133] emphasized the

change of thermal conductivity with temperature. Guo et al. [134] mentioned that the effect of size and temperature of the wood pellets are insignificant towards thermal conductivity, in contrast with the impact of the structure of the wood. While the influence of temperature is debatable in the literature, the importance of structure has been accentuated repeatedly [90, 134, 135]. However, researchers tend to ignore the mentioned results and use the same value for thermal conductivity for different wood species [90].

For calculation of ETC for WPCs, polymer characteristics, wood particles and the interaction between these two phases need to be considered [136]. Wood ETC depends on its physical and chemical properties such as the percentage of cellulose, lignin, moisture content, and fiber orientation, as the difference can be seen in Table 3.1. Shebani et al. [136] stated that a notable variation is produced through changing the type of wood species. He observed that with a higher cellulose content, the system has superior thermal stability. Moisture content is another essential parameter for the ETC, as higher moisture content results in higher thermal conductivity [137]. It has been shown that fiber structure remains the same after devolatilization [138], which is of importance where the basis of the model is on raw material. Finally, increasing the temperature results in higher thermal conductivity of the wood [139]. As for the plastic, popular polymers in the industry such as polyethylene (PE), polypropylene (PP), polyvinyl chloride (PVC) or polyamide have high thermal resistance and therefore are mainly used as thermal insulators [140, 141]. HDPE is reported to have the highest thermal conductivity, and PI has the lowest value [142]. Crystallinity is a significant parameter that affects the thermal conductivity of polymers, with higher crystallinity resulting in higher thermal conductivity [142]. Chen et al. [142] pointed out the exception of this relation which is PP, a highly crystalline polymer with low thermal conductivity. In contrast with wood, polymers tend to have lower thermal conductivity with increasing temperature [139]. Charring polymers such as poly(ethylene terephthalate) (PET) have a different thermal conductivity at different states of gasification such as melt and char compare to raw material [143].

Kumlutas et al. [140] mentioned two methods for improving the thermal conductivity of polymers. The first approach is by changing the molecular orientation where parallel orientation results in better thermal conduction. This method is highly effective but not always possible and is relatively costly. The second technique is to add conductive fillers such as short fibers which is

a more accessible method for increasing ETC. Agoua et al. [144] tested the effect of adding a glue made of PS to wood composite and observed higher thermal conductivity with the increase of PS content, in addition to reducing pores. Ndiaye et al. [145] observed disruption of the homogenous structure of pure PP by adding wood flour as a filler, as a result of interfacial debonding that voids and fiber exhibit in the matrix. In the case of WPC made of HDPE and wood flour, the thermal conductivity is reduced by increasing temperature and wood flour content [139]. Finally, adding biochar to WPCs reduces the surface roughness and improves thermal conductivity [146]. Das et al. [146] concluded that since biochar has relatively smaller particles, increasing biochar loading rate enhanced interconnecting network inside the matrix and resulted in a good dispersion and lower interfacial thermal resistance. They suggested that for high temperature similar to gasification range, there is a possibility of increased crystallinity of biochar which will further improve thermal conductivity.

In the analytical calculation of ETC, most common methods are based on a simple averaging by using volume fraction as the weight parameters. However, errors as high as 20% have been reported with averaging methods [147]. An extended version of Maxwell [148] and Rayleigh [149] formula for electrical conductivity of uniform spheres of one material in a cubic array of another phase in a two-phase medium is also a common approach for the calculation of thermal conductivity. As stated by Woodside et al. [150], the problem with this approach is the limitation of the porosity range, which was found to be a maximum of 0.5, whereas, for a material such as wood char, the porosity can go as high as 0.8. Siau et al. [12] and Saastamoinen et al. [151] used the resistance analogy to electrical conductivity by separating the wood structure to layers in parallel and series. Their results had underestimation and overestimation error, according to [138]. Thunman et al. [138] combined these two models to modify the result. However, the model is suited for a specific range of density, and there is a 15% error for fuel with high density such as pellets. The calculations become more inaccurate and complicated for WPCs due to the addition of a plastic phase in the structure.

As a result of the imprecision of the analytical methods for calculating thermal conductivity, literature has shifted toward computational methods that provide a more precise insight into the matter. Consequently, application of the discretization methods such as the finite element method (FEM), finite volume method (FVM) and finite difference method (FDM) has increased

tremendously in the literature. Andmi et al. [152] pointed out that the FEM is more suitable for complex systems since it is not restricted by regular nodes positioning, whereas FDM is less time consuming and suitable for simpler models. The FVM is used mostly for macroscopic analysis such as in ETC in lumber [153] which is not the focus of this study.

FEM has been one of the most popular methods for calculation of ETC of composites and nanocomposites of different materials [140, 154-157]. Staggs et al. [158] used FEM alongside a thermal conductivity sub-model and an attractive digital image method for pore size distribution, in order to calculate ETC of a 2D and 3D char structure. In their model, a digital image is converted to a black and white image and each pixel of the latter form is designated to either char or pores based on the color being black or white, respectively. The result is then put in a matrix for FEM and further used to calculate steady temperature equation, heat flux and consequently ETC for 2D char. The 3D calculations were based on 2D results and assuming spherical geometry for pores. The results were compared to two exact solutions and showed high accuracy despite the simplifying assumptions. El Moumen et al. [159] implemented FEM with homogenization to replace analytical method of defining boundaries for ETC values. The model was considered a 2D porous volume with a random distribution of identical spherical or ellipsoidal pores and the FEM was used to examine the effect of pores arrangement in the structure of the material. These models show an enhanced result over analytical methods, in addition to lowering the assumptions, thus providing a suitable replacement for conventional models.

The number of computational models dedicated to ETC of WPCs is scarce in the literature. FEM and FVM are used among the few models that exist in the literature, such as [152] and [160], respectively. According to Aadmi et al. [152], FEM is applicable for WPC as long as the inhomogeneities are insignificant compared to the dimensions of the object, thus making it possible to spatially average heat conduction across the system and define a uniform ETC. Aadmi et al. [152] found replacing analytical methods with FEM to create a 3D model to predict ETC of composites strengthen the predictions and stability of the model. They coupled the model with a program for generating forms reinforced with randomly distributed inclusion such as spherical, cylindrical and ellipsoidal to find the effect of shape and size of inclusions. The results show that ellipsoidal inclusion and smallest fillers produce the highest ETC and were justified by comparison with two analytical methods, namely Hasin -Shtrikman and Hatta-Taya, with a maximum of 5%

error. Bourai et al. [160] used two-dimensional FVM to find the effect of concentration of wood and temperature on the WTC of WPCs, whereas the WPC is a mixture of LMDPE and pine wood particles with a random distribution. The model was fixed between upper and lower boundaries that belong to parallel and perpendicular orientation, respectively and the binary system was considered without the existence of porosity. They used low wood content (0-20%) and found out that ETC decreases by increasing wood concentration. As mentioned before, FVM is not suitable for microscopic analysis which is required with a high concentration of inclusion, as well as randomly fiber orientation. Therefore, by increasing the wood content, the result of the model showed inconsistencies with analytical data.

There is an insufficiency of research done in the modeling of ETC of WPCs with consideration of all the phases in the system and high-temperature range. Regarding the potential that computational models have in computing ETC, the next section is devoted to providing a novel FEM homogenization model to examine the effect of adding plastic to wood pellets and calculate the ETC of such WPCs.

Table 3.1: ETC of composites based on polymer loading (PL) (Dry Basis)

Ref.	Type of wood	Type of plastic	keff
[144]	Wastes of wood of Kaya senegalensis	Expanded polystyrene	0.263 W/(m °C).
[144]	Pterocarpus erinaceus	Expanded polystyrene	0.242 W/(m °C).
[137]	Simul (Salmalia malabarica)	butylmethacrylate (BMA)	0.062 (PL=38%) W/m C
[137]	Simul (Salmalia malabarica)	methylmethacrylate (MMA)	(PL=0.45%) 0.057 W/m C
[137]	Mango (Mangifera indica)	butylmethacrylate (BMA)	(PL=31%) 0.047 W/m C
[137]	Mango (<i>Mangifera</i> indica)	methylmethacrylate (MMA)	0.052 W/m C
[146]	Pine wood	PP composite (WPC)	0.1883 W/m.K

3. 2. Methodology

Studying the thermal behavior of complex materials such as composites requires knowledge of their microstructure and its relation to the whole body of the material. Therefore, a unit cell (UC) or representative volume element (RVE) is defined, assuming that RVE has a periodic behavior along the surface of the structure, thus resulting in the periodic behavior of any function defined in the microstructure boundaries [161]. It has been repeatedly pointed out in the literature that RVE can only be applied as a microstructure as long as it has relatively small size compared to the macro-sized element [161-164]. As the next step, the properties that need to be studied are divided into local and global levels devoted to microstructure and macrostructure analysis, respectively and their mathematical relation is investigated while using periodic boundary conditions related to RVE [165]. In case of the effective properties, the RVE is considered homogenous and thus leads to replacing the heterogeneous composite with a periodic system that represents its effective properties, which is called homogenization [162]. Furthermore, homogenization methods that use the asymptotic expansion of the governing equations are called asymptotic expansion homogenization (AEH).

Here, we have used AEH with the conjunction of FEM to solve the differential equations, which is referred to as numerical homogenization [163], in order to derive out effective thermal conductivity (ETC) of WPCs. The WPC used here is considered to have porous wood-char as the matrix and HDPE as the plastic inclusion. This method can be implemented for analysis of the gasification of feedstocks, since there is an evident lack of data for higher temperature range after pyrolysis and specifically for composites such as WPCs. The AEH formulas for thermal conduction are derived from Song et al. [164] since it considers three phases, while similar equations can be found in [163, 166, 167]. ANSYS software was used to carry out the FEM calculation. Model description and solution procedure are further discussed in this section.

3. 2. 1 Model description

The governing equation is defined for each phase based on the Fourier's law and steady-state heat conduction assuming insignificant heat generation [49]:

$$-\frac{\partial}{\partial x_i} \left(k_{ij}^w \frac{\partial T}{\partial x_j} \right) = 0 \text{ in } \Omega_w \tag{3.1}$$

$$-\frac{\partial}{\partial x_i} \left(k_{ij}^p \frac{\partial T}{\partial x_j} \right) = 0 \text{ in } \Omega_p$$
(3.2)

$$-\frac{\partial}{\partial x_i} \left(k_{ij}^a \frac{\partial T}{\partial x_j} \right) = 0 \text{ in } \Omega_a$$
(3.3)

where k_{ij}^w , k_{ij}^p and k_{ij}^a are the second-order thermal conductivity tensors for wood, plastic and air, respectively. In additon, asymptotical expansion of temperature field has been formulated in equation (3.4):

$$T(x_i, y_i) = T^{(0)}(x_i, y_i) + \varepsilon T^{(1)}(x_i, y_i) + \varepsilon^2 T^{(2)}(x_i, y_i) + \cdots$$
(3.4)

where x_i and y_i are used to define the global and local length scales. In addition, ε represents the relation between x_i and y_i as follow:

$$y_i = \frac{x_i}{\varepsilon} \tag{3.5}$$

Furthermore, $T^{(1)}$ is defined based on equation (3.6):

$$T^{(1)}(x_i, y_i) = -\chi_j(y_i) \frac{\partial T^{(0)}}{\partial x_i}(x_i) + \tilde{T}^{(1)}(x_i)$$
(3.6)

where χ_j is defined as an arbitrary characteristic function which is only dependent on y_i the coordinate system, as compare to x_i coordinate system. By replacing differentiating operator based on equation (3.5), writing expansion of equation (3.1) to (3.3) by order of ε , and finally implementing equation (3.6), equations (3.1) to (3.3) are rewritten as follow:

$$-\frac{\partial}{\partial y_i} \left(k_{ik}^w \frac{\partial \chi_j}{\partial y_k} \right) = -\frac{\partial}{\partial y_i} k_{ik}^w \text{ in } \Omega_w$$
 (3.7)

$$-\frac{\partial}{\partial y_i} \left(k_{ik}^p \frac{\partial \chi_j}{\partial y_k} \right) = -\frac{\partial}{\partial y_i} k_{ik}^p \quad in \quad \Omega_p$$
(3.8)

$$-\frac{\partial}{\partial y_i} \left(k_{ik}^a \frac{\partial \chi_j}{\partial y_k} \right) = -\frac{\partial}{\partial y_i} k_{ik}^a \text{ in } \Omega_a$$
(3.9)

Finally, the conductivity tensor over the whole domain or Ω is integrated and results in the homogenized effective conductivity tensor:

$$\langle k_{ij} \rangle = \frac{1}{\Omega} \int (k_{ij} - k_{ik} \frac{\partial \chi_j}{\partial y_k}) dy$$
 (3.10)

3. 2. 2 Solution Procedure

The FEM-based ANSYS calculation is used to solve equation (3.10) for various filler concentrations with mesh sensitivity of 8×50,000. RVE used in this model is defined as three-dimensional concentric cubes in the cube to represent each phase as in Figure 3.1.

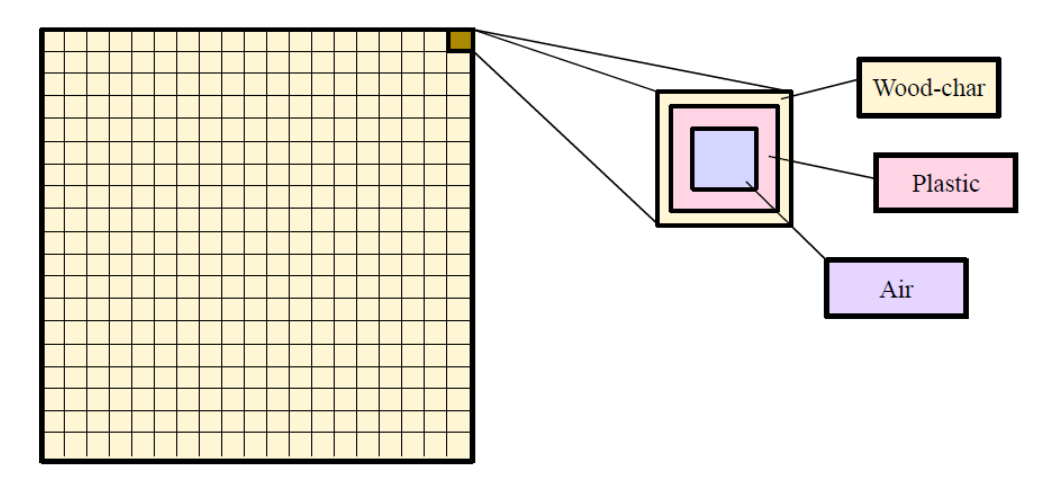


Figure 3.1: Quadratic RVE of three-phase WPC, wood-char, plastic and air. The phases are considered as concentric cubes inside each other.

To validate the numerical model, the exact values for upper and lower bound corresponding to the parallel and series placement of phases were calculated as follow [160]:

Upper bound:
$$\frac{1}{k_c} = \frac{\phi_w}{k_w} + \frac{\phi_p}{k_p} + \frac{\phi_a}{k_a}$$
 (3.11)

Lower bound:
$$k_c = k_w \phi_w + k_p \phi_p + k_a \phi_a$$
 (3.12)

where k_c is the ETC of composite and k_w , k_p and k_a are the thermal conductivity of wood-char, plastic and air, respectively. Moreover, ϕ represents the volume fraction of each phase. Three

phases of non-porous wood-char, HDPE and air have been considered and their thermal conductivities are collected in Table 3.2:

Table 3.2: Thermal conductivity of different phases of modeled WPC

Material	Thermal conductivity	Reference
	W/m-K	
Non-porous char	1.85	[168]
HDPE	0.43	[142]
Air	0.071	[168]

Non-porous wood char was chosen instead of wood, for the fact that char has lower interfacial thermal resistance with plastic as discussed in thermal conductivity section. Thus, the computational model will have higher accuracy when compared to experimental data. The purpose of the model is to be implemented for the gasification process, making char a more suitable option. As for the polymer, HDPE is selected because of its relatively high thermal conductivity compared to the other polymers, as well as its abundance in recyclable waste.

3. 3. Results and discussion

The calculation of ETC has been carried out for the HDPE and wood-char with different level of porosity, as well as three relative volumes of 0.1, 0.3 and 0.5 of HDPE to wood-char for a WPC demonstrated in Figure 3.2 and Figure 3.3, respectively.

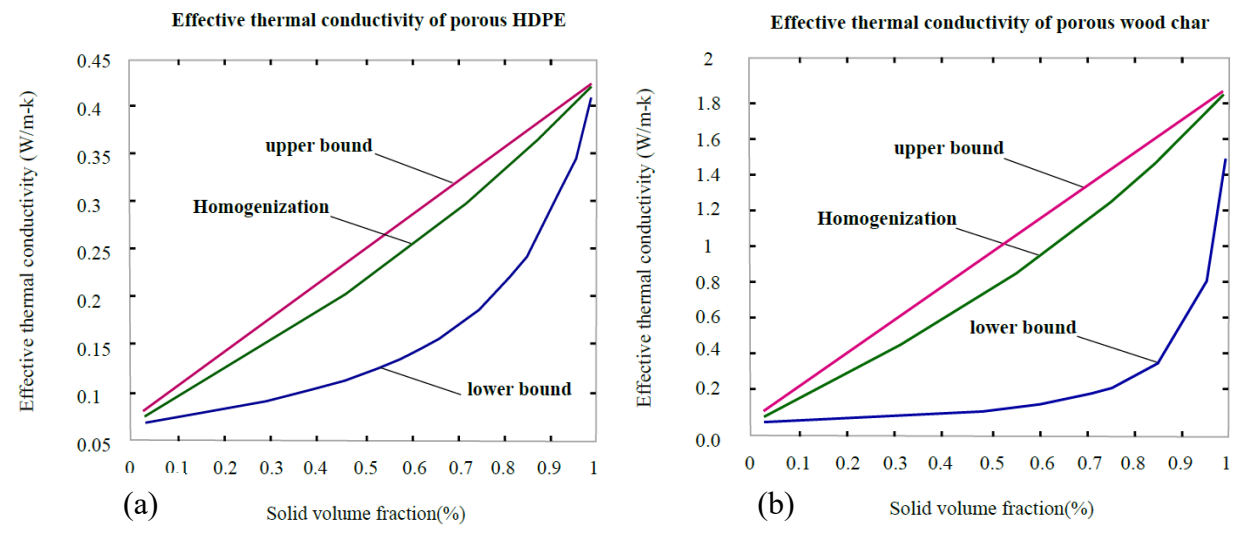


Figure 3.2: result of estimating thermal conductivity of a) porous HDPE b) porous wood char with homogenization and the upper and lower bound calculations

As expected, Figure 3.2 shows that by increasing the percentage of solid volume fraction or decreasing porosity for either of HDPE and wood-char, the ETC is increasing. This trend can be explained by the relatively low thermal conductivity of the gas compared to both HDPE and wood char. Subsequently, by increasing solid volume fraction, gas component becomes smaller, and higher ETC is observed. Comparison between part (a) and (b) of Fig.3.2 shows a higher rate for wood-char than HDPE as a result of increasing solid volume fraction. With superior thermal conduction of wood-char, increasing solid volume fraction results in higher overall conduction and thus homogenization results show more significant divergence from lower bound in part (b) compare to part (a). This trend is also observed for Figure 3.3 by showing the effect of increasing HDPE volume to wood-char on the overall ETC of WPC. By replacing the wood-char with HDPE with the same solid volume fraction in the composite, the ETC is decreasing, and the reduction intensifies as the solid volume fraction reaches unity in the structure of WPC. This behavior is justified by the same logic that supported the trend of Figure 3.2, the difference between the thermal conductivity of wood-char which is 1.85 W/m-K, more than four times larger than the thermal conductivity of HDPE, 0.43 W/m-K. However, for the composites that the addition of plastic is aiming for higher thermal conductivity, the experiment is designed in a way that HDPE is filling the pores of the wood, not replacing the wood volume. Thus, it is necessary to consider the change of solid volume fraction while evaluating ETC of the product. To illustrate, consider a simple example: if the feedstock is a WPC with plastic to wood ratio of 0.1, solid volume percentage of 0.5 and we consider the total volume to be constant and equal to 1, the volume of gas can be calculated as follow:

$$\frac{V_p}{V_w} = 0.1$$
 plastic to wood ratio of feedstock $\rightarrow V_p = 0.1 V_w$
 $V_t = V_p + V_w + V_a = 1$ total volume of plastic, wood, and air is considered equal to 1

 $V_s = V_p + V_w = 0.5$ total solid volume (solid volume fraction is 0.5 and total volume is 1)

 $\rightarrow V_s = 1.1 V_w = 0.5 \rightarrow V_w = \frac{0.5}{1.1} = 0.45 \rightarrow V_p = V_s - V_w = 0.045$
 $V_a = V_t - V_s = 0.5$

Next, we add HDPE filler to the above WPC until we reach a plastic to wood ratio of 0.3. If we consider the wood-char volume constant, HDPE is filling the pores and increasing solid volume fraction. Then we have:

$$\frac{V_{p,new}}{V_w} = 0.3$$
 solid volume fraction of the product $V_w = 0.45$ constant wood-char volume $\rightarrow V_{p,new} = 0.3 \times 0.45 = 0.135$ $\rightarrow V_s = V_{p,new} + V_w = 0.135 + 0.45 = 0.585$

The difference between the initial plastic volume and final is the reduction of pores in composite:

$$V_a - V_{a,new} = V_{p,new} - V_p = 0.135 - 0.045 = 0.09$$
 3.13

Therefore, the ETC of 0.1 ratio in 50% solid volume fraction of feedstock needs to be compared with 0.3 ratio in 58% for the product.

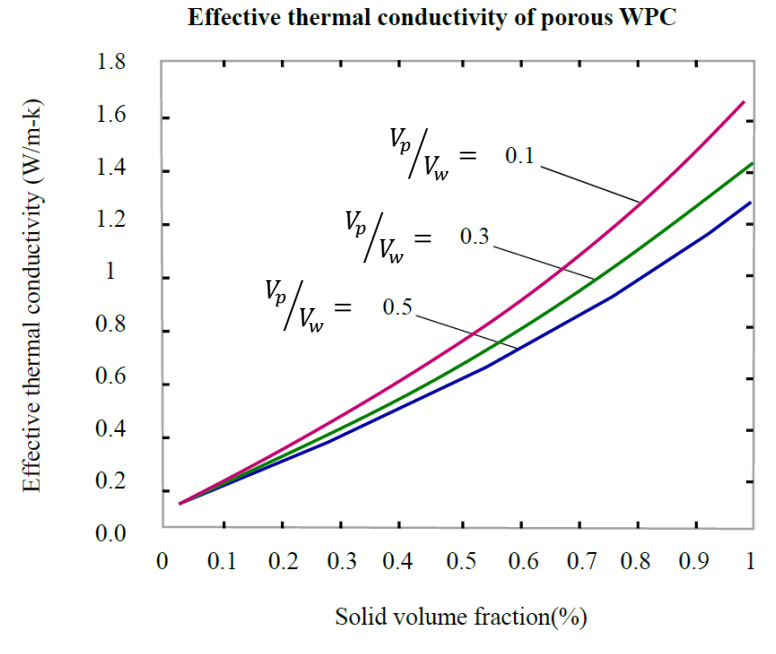


Figure 3.3: effect of solid volume fraction and ratio of HDPE to plastic on ETC of WPC

Figure 3.4 is illustrated to show the validity of calculations by using the upper and lower bound. As it can be observed, all the values derived out from the model fall between the upper and lower bound data. As the solid volume percentage goes higher, the ETC estimated by homogenization

model gets further from lower bound and more inclined to higher bound and as solid volume fraction gets closer to zero, the difference between the value of ETC and lower bound becomes smaller. Both behaviors are a direct outcome of low thermal conductivity of air, so the more gaseous volume results in closer ETC to lower bound, whereas before 0.1% solid volume fraction the difference is insignificant. Moreover, the highest upper bound is for 0.1 plastic to wood ratio, and the lower upper bound is for 0.5 plastic to wood ratio because of the higher thermal conductivity of wood-char compared to plastic.

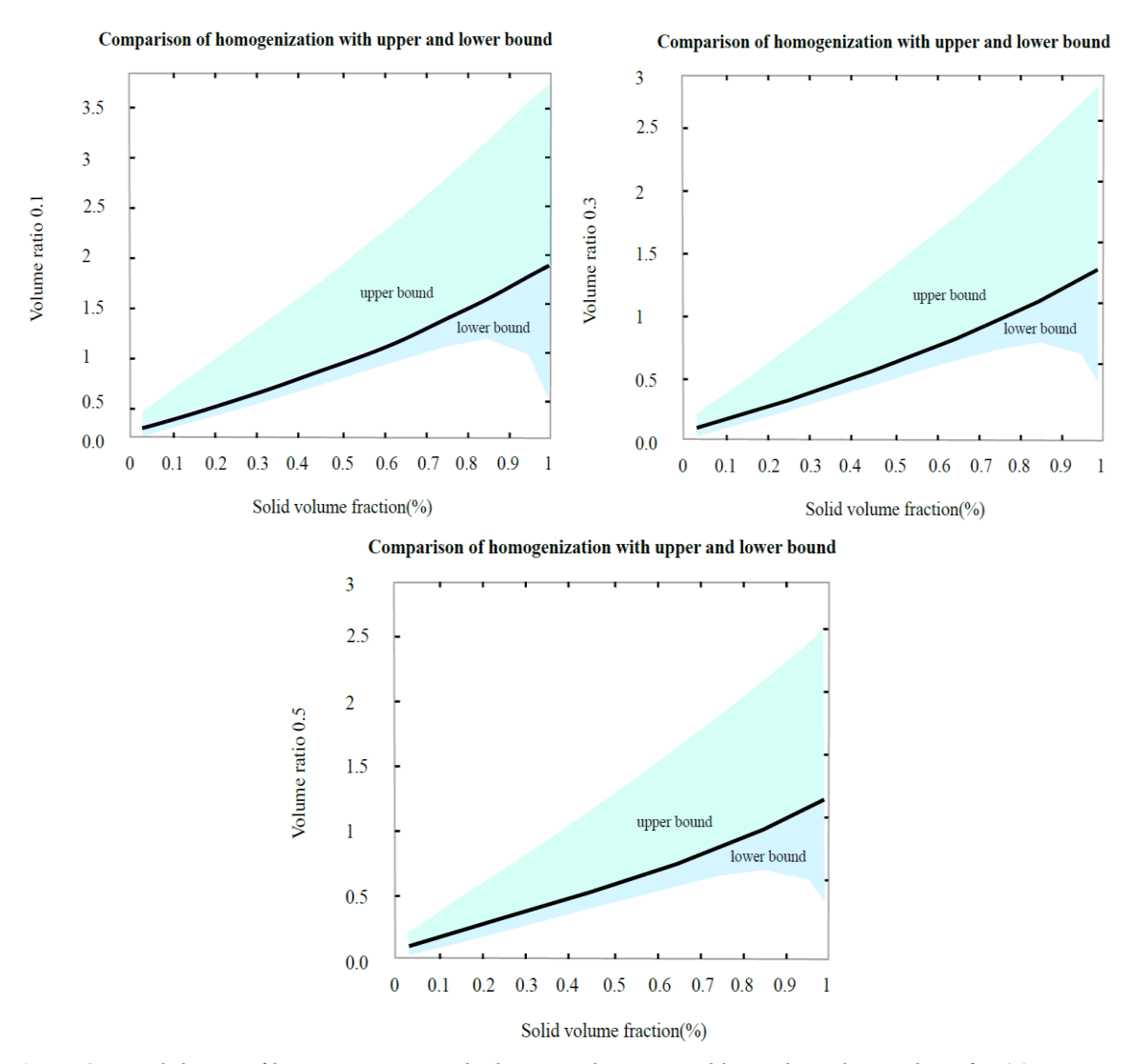


Figure 3.4: Validation of homogenization calculation with upper and lower bound error bars for (a) 0.1, (b) 0.3 and (c) 0.5 volume ratio

3. 4. Conclusions

In this study, the trends of ETC for WPCs made of HDPE and wood-char with different solid volume ratio, and 0.1, 0.3 and 0.5 plastic to wood ratios have been evaluated. The homogenization method with FEM-based solver ANSYS was used, and the results were validated by calculating the upper and lower bound for parallel and series placements of three phases. Higher solid volume fraction and lower plastic to wood ratio resulted in better thermal conductivity for WPC. These results can be further used to study gasification of WPCs, by modeling the porosity development where the analytical data for changes of ETC with temperature is not available. In addition, it can be used to test the behavior of different mixtures of WPC based on the solid volume fraction and inclusion to matrix ratio. Therefore, homogenization has been proven to be a useful tool to estimate the change in ETC with minimum limitation compared to other methods. However, there is still a lack of knowledge for higher temperature behavior of WPCs and experiments need to be done in order to validate the computational data for gasification purposes.

3. 5. Connecting statement

In Chapter 3, a homogenization model was developed to estimate the effective thermal conductivity of WPC which is a possible feedstock for the gasifier. If the validity of the behavior of polymer in temperatures higher than 800K is studied, the result of homogenization model can be used directly in the next numerical method, which is a 1D gasification model for the wood particle. Both models are beneficial to provide additional knowledge prior to carrying out experiments.

CHAPTER 4: One-dimensional modeling of gasification in woody biomass particle

One-dimensional modeling of gasification in woody biomass particles

N. Mazaheri, A.H. Akbarzadeh, M. Lefsrud

Department of Bioresource Engineering, McGill University, Ste-Anne-de Bellevue, QC H9X 3V9. Canada

Abstract

The purpose of this study is to conduct a preliminary one-dimensional (1D) modeling for gasification of a single pellet of woody biomass in a downdraft gasifier, to test the model and compare the results of the modeling with the trend of analytical data available in the literature. This modeling is specified to oxidation and reduction reactions of char particle after a complete pyrolysis, which consists of both gas and solid phases. Heat transfer studies are added in the form of conduction, as well as mass transfer. Kinetics equation is used to calculate the rate of reactions used for determination of temperature distribution. The numerical model requires physical and chemical properties of char and ambient gas phase as an input to provide temperature profile across the radius of the particle as an output of the model. The *pdepe* built-in function of MATLAB has been used to solve the parabolic 1D conservation equations. The temperature first increases rapidly and then reaches a steady state passing 3000s. The temperature on the radii closer to the surface has a higher temperature compared to the core. An extensive temperature distribution graph is demonstrated by time and radius.

4. 1. Introduction

The gasification is a complicated process, following four main steps which include: (1) drying, (2) pyrolysis, (3) partial combustion of the gasses, vapors and the char, and (4) reduction of the combustion products. The temperature increases with the radius, as it can be seen in Figure 2.7 in chapter 2. As the biomass undergoes the pyrolysis process, the char is produced and the porosity increases. Since the surface of the particle is exposed to the heat produced during the reactions and the radiation (due to the high temperature of the other particles), it has a higher temperature compared to the temperature within the particle. The radius of the biomass is one of the main parameters to determine the existence of a temperature gradient inside the particle. For microscopic particles, we can acknowledge a lumped element model. A lumped element model considers a constant temperature within the volume of the element[90]. However, the feedstock biomass for downdraft gasifiers is not small enough to neglect the temperature gradient existing inside the particle, thus falling into the thermally-thick regime.

One of the most critical challenges during the modeling of the gasification process is biomass pyrolysis, and char reactions can happen at the same time. In a conventional gasifier, before complete pyrolysis of the biomass, char starts reacting with the gases existing in the pores due to the high temperature on the outside layers of the particle, while inside the particle biomass is still producing the chars in the pyrolysis process. Therefore, here the ideal complete pyrolysis is considered, and the focus of the model is only on the char reactions.

4. 2. Methodology

4. 2. 1 Model description

The initial condition for the modeling is applied when the biomass has gone through the drying and complete pyrolysis processes leading to production of the char and the volatiles. As the next step, the char reacts with the volatiles and air components within the pores of char. The change in the temperature of the syngas is the output of this model. The change is only considered along with the radius and time and following general assumptions are used for simplification:

- 1. Symmetric
- 2. Unsteady
- 3. 1D
- 4. Constant surface radius (the particle is not shrinking)
- 5. Ideal gas
- 6. The constant density of the char and the volatiles which means the average density changes by the porosity alone.
- 7. No pressure gradient is considered inside the particle since a high initial porosity is considered. The small porosities lead to a pressure gradient through the pore, but the pressure through the pores with the conversion (gasification of the wood char).
- 8. Nu = 2 which affects B0 for the equations 4.16 and 4.17 on the surface of the particle. This is for the case of free convection, and we are considering no presence of the forced convection.
- 9. For deriving constants of each reaction, the data for 10% conversion have been used by Dasappa et al. [117].

In the next section, the details of each equation used along with the choices of the variables are described.

4. 2. 2. Equations

The conservation equation is extended versions of the Equation (4.1):

$$\frac{d}{dt} \int_{V} \Phi dV = -\int_{S} F. dS - \int_{S} \Phi_{V}. dS + \int_{V} H dV$$
 (4.1)

where ϕ is any quantity that changes within the volume element (dV), F is the flux vector of ϕ quantity in the absence of fluid transport, $\phi_{\mathbf{V}}$ is the transport flux vector (per unit area per unit time), S is the surface vector perpendicular to the flux direction and H is the source term. If we consider the surface and volume fixed in the inertial frame, we will have:

$$\frac{d}{dt} \int_{V} \Phi dV = \int_{V} \frac{\partial \Phi}{\partial t} dV \tag{4.2}$$

Integrating Eq. (4.1) results in:

$$\frac{\partial \Phi}{\partial t} + \nabla \cdot (\mathbf{F} + \Phi_{\mathbf{V}}) - H = 0 \tag{4.3}$$

Equation (4.3) is used for the mass, energy, and concentration conservation equations in 1D (radial direction) spherical coordinates. The following equations are adapted from Dasappa et al. [44, 51, 90, 117]:

• Mass conservation for gas phase:

$$\frac{\partial}{\partial t}(\rho\epsilon) = \frac{1}{r^2} \frac{\partial}{\partial r} (-\rho v r^2) + \dot{\varpi}_c''' \tag{4.4}$$

As it can be seen, the term on the left-hand side shows the change in density of the gas. The first term on the right is the flux of gas leaving the pores of the char as reaction happens and the second term is the gasification rate of char showing the rate of mass production.

• Energy conservation:

$$\frac{\partial}{\partial t} (\rho C_p T) = \frac{1}{r^2} \frac{\partial}{\partial r} \left(-\rho v r^2 C_p T + r^2 \kappa \frac{\partial T}{\partial r} \right) - H_c \dot{\varpi}_c^{""}$$
(4.5)

In energy conservation equation, the first right term is the energy syngas carries out of the pores and the second term is the conduction term. The third term is the energy produced through reaction, and it is calculated by multiplying enthalpy of char and gasification rate.

• Porosity

$$\frac{\partial \epsilon}{\partial t} = -\frac{\dot{\varpi}_c'''}{\rho_c} \tag{4.6}$$

This equation is based on Howard [169] equation for the tube-shaped pores in the particle and shows the change of porosity with time.

4. 2. 3. Reactions

Through the gasification, many reactions happen, as it can be seen in Table 4.1 [15]. Here the aim is to focus on the modeling and considering all the reactions results in time-consuming and limited analysis. Thus, the three primary reactions of the char with O_2 , CO_2 , H_2O are considered. These reactions are used to calculate $\dot{\varpi}_c'''$ and consequently temperature distribution in particle.

Table 4.1: Summary of the fundamental reactions in the gasification process of biomass [15].

Fundamental Reactions in the
gasification
$C < S > +0.5O_2 = CO$
$C < S > + CO_2 = 2CO$
$C < S > + H_2O = CO + H_2$
$CO + 0.5O_2 = CO_2$
$H_2 + 0.5O_2 = H_2O$
$CO + H_2O = CO_2 + H_2$
$CO_2 + H_2 = CO + H_2O$
$CH_4 + O_2 = CO_2 + 2H_2O$
$CH_4 + H_2O = CO + 3H_2$
$CO + 3H_2 = CH_4 + H_2O$

Copyright has been granted by publisher

• **Reaction** *C* + *O*₂ [168, 169]:

$$\dot{\omega}_{c+O_2}^{"} = -\frac{M_c S_1 S_2 X_{os}}{(S_1 X_{os} + S_2)} \tag{4.7}$$

$$S_1 = \frac{A_c Pexp\left(-\frac{E_1}{RT}\right)}{\sqrt{2\pi M_{O_2}RT}}: \text{ rate constant for absorption}$$
 (4.8)

$$S_2 = A_f exp\left(-\frac{E_2}{RT}\right)$$
: rate constant for desorption (4.9)

$$\dot{\omega}_c^{"'} = \dot{\omega}_{c+o2}^{"} * S_g * \rho_{ap} \tag{4.10}$$

$$S_g * \rho_{ap} = \frac{2\epsilon}{r_p} \tag{4.11}$$

$$\dot{\omega}_{c+o_2}^{""} = \frac{2 * \dot{\omega}_{c+o_2}^{"} \epsilon}{r_p} \tag{4.12}$$

These equations are initially provided by Howard [169] to describe the volumetric rate of reaction for the carbon content of char and oxygen. The constants have been calculated from the data of 10% conversion of char [117] as mentioned earlier assumptions and are summarized in Table 4.2. It should be mentioned that M_c is carbon molecular mass which has a value of $12.001 \times 10^{-3} \frac{kg}{mol}$.

Constants for the reaction of char and oxygen					
A_c	$\frac{E_1}{R}$	$\frac{E_2}{R}$	A_f	r_p	Xos
$\frac{1}{150}$	1700 K	20,000 K	$0.0875 \frac{mol}{m^2 - s}$	$5 \times 10^{-5} m$	0.21

Table 4.2: Constants for the reaction of char and oxygen

It is worth mentioning that X_{OS} is the mole fraction of oxygen at the surface and is based on the air flux concentration of the oxygen. Since we have the concentration based on the mass fraction, the conversion is calculated as follow:

$$x_i = \frac{\frac{m_i}{M_i} \times \frac{1}{m_t}}{\sum \frac{m_i}{M_i} \times \frac{1}{m_t}} = \frac{\frac{Y_i}{M_i}}{\sum \frac{Y_i}{M_i}}$$

• **Reaction** *C* + *CO*₂ [168]

$$\dot{\omega}_{C+CO_2}^{\prime\prime\prime} = -M_c \frac{k_1 p_{CO_2} - k_2 p_{CO}^2}{1 + k_3 p_{CO} + k_4 p_{CO_2}} \tag{4.13}$$

This rate equation is reported by Semechkova and Frank-Kamenetski [170], and it is only acceptable at the atmospheric temperature. As provided in Table 4.3, the constants for equation 4.13 are given by Dasappa et al. [168] and k_2 is calculated from their experimental data.

Table 4.3: Constants for reaction of char and carbon dioxide [168]

Co	Constants for the reaction of char and carbon dioxide		
k_1	$2.2*10^{9} \exp\left(\frac{-E}{RT}\right) \frac{mol}{cm^{3} - s - atm}$		
1	E= 293 kJ/mol		
k_2	$24.38 \times 10^{-6} \frac{mol}{m^3 - s - atm^2}$		
k_3	$15 atm^{-1}$		
k_4	$0.25 \ atm^{-1}$		

• Reaction $C + H_2 O$ [117]

$$\dot{\omega}_{C+H_2O}^{""} = -M_c \frac{k_1 p_{H_2O} + k_4 p_{H_2} p_{H_2O} + k_5 p_{H_2O}^2}{1 + k_2 p_{H_2} + k_3 p_{H_2O}}$$
(4.14)

This reaction is by Blackwood and McGory[117], and the constants are as follow:

Table 4.4: constants for char and water vapor reaction [117]

Con	Constants for char and water vapor reaction		
k_1	$3.7 \times 10^7 \exp\left(-\frac{30,000}{T}\right) \frac{mol}{cm^3 atm}$		
k_2	$35 \ atm^{-1}$		
k_3	$2.1 \times 10^{-3} exp\left(-\frac{10,055}{T}\right) atm^{-1}$		
k_4	91.8 $exp\left(-\frac{15,083}{T}\right) atm^{-1}$		
k_5	$2.5 \times 10^{-8} \ atm^{-1}$		

4. 2. 4. Initial and boundary conditions

As for initial conditions, the temperature and concentration of each gas depend on the experimental setup. However, we make certain assumptions to simplify the modeling procedure. The initial temperature in this model is set to 800K. The boundary conditions are considered between surface and infinity. At infinity, the gas phase is considered as air mass fractions [171], and the temperature is 1200K. For the surface, we consider the quasi-steady gas phase and solve Equation 4.5 and 4.6, and by considering the Lewis number as one the result is as follow:

$$\frac{(T - T_{\infty})}{(T_s - T_{\infty})} = \frac{(Y_i - Y_{i\infty})}{(Y_{is} - Y_{i\infty})} = \frac{(1 - \eta)}{(1 - \eta_s)}$$
(4.15)

where $\eta_S = \exp(-\frac{\dot{m}c_p}{4\pi k r_S})$ and $\eta = \exp(-\frac{\dot{m}c_p}{4\pi k r})$. As the next step by differentiating solution at the surface radius, the boundary condition for concentration as well as temperature is found:

$$k\frac{\partial T}{\partial r} = C_P Q(T_\infty - T_S) - \dot{R}'' \tag{4.16}$$

$$D \rho \frac{\partial Y_i}{\partial r} = Q(Y_{i\infty} - Y_{is})$$
(4.17)

where $Q = \left[\frac{\dot{m}}{4\pi r_s^2} \frac{\exp(-B_0)}{\{1 - \exp(-B_0)\}}\right]$ and $B_0 = \frac{\dot{m}c_p}{4\pi k r_s}$. The air mass fraction and syngas mass fraction equilibrium modeling result are both summarized in Table 4.5.

Table 4.5: Gas composition for boundary conditions

Gas component	Air (%) [171]	Syngas(%) [33]
N ₂	75.47	59.1
O_2	23.20	-
CO_2	0.0062	8.5
СО	-	18.9
H_2	-	12.5
CH ₄	-	1.20

The partial pressure is needed to use gas components for the reaction rate and can be calculated using PV = nRT as follow:

$$\frac{p_i}{p_t} = \frac{n_i}{n_t} = x_i \to p_i = p \times x_i \tag{4.18}$$

where p_i is partial pressure of the ith gas component in the gas phase and n_i is a number of moles of ith component. The summarized partial pressures used in the calculations are given in Table 4.6.

Mole fraction	Partial pressure (atm)
$x_{H_2} = 12.5/100$	$p_{H_2} = 0.009$
$x_{\rm CO} = 18.90/100$	$p_{\rm CO} = 0.2$
$x_{\text{C}H_4} = 1.2/100$	$p_{\mathrm{C}H_4} = 0.010$
$x_{CO_2} = 8.5/100$	$p_{CO_2} = 0.142$
$x_{N_2} = 59.10/100$	$p_{N_2} = 0.513$
$x_{H_2O} = 0.00943864$	$p_{H_2O}=9.3*10^{-5}$

Table 4.6: Partial pressure of gas phase components

4. 2. 5 Solution Procedure

The MATLAB built-in function pdepe has been used to solve the parabolic 1D equations with 100 mesh points, the porosity of 88%, the initial temperature of 800K and the infinity temperature of 1200K. The pdpe function uses the finite element method (FEM) to solve the equations. The form of pdepe is as follow:

$$c\left(x,t,u,\frac{\partial u}{\partial x}\right)\frac{\partial u}{\partial t} = x^{-m}\frac{\partial}{\partial x}\left(x^{m}f\left(x,t,u,\frac{\partial u}{\partial x}\right)\right) + s\left(x,t,u,\frac{\partial u}{\partial x}\right) \tag{4.19}$$

where f is the flux and s is the source term. If we write the Equations 4.5 and 4.6 in the form of Equation 4.20, we have:

$$\bar{\rho}C_{p}\frac{\partial}{\partial t}(T) = \frac{1}{r^{2}}\frac{\partial}{\partial r}\left(r^{2}\left(-\rho vC_{p}T + \kappa \frac{\partial T}{\partial r}\right)\right) - H_{c}\dot{\varpi}_{c}^{"'}$$
(4.20)

The boundary conditions are in the form of Equation 4.21:

$$p(x,t,u) + q(x,t)f\left(x,t,u,\frac{\partial u}{\partial x}\right) = 0 (4.21)$$

As mentioned before, the Equation 4.19 and 4.20 are the boundary conditions considered in these modeling. If we turn those equations into the form of Equation 4.21, Equation 4.22 and 4.23 will be the results:

$$C_P Q(T_\infty - T_S) - \dot{R}'' + k \frac{\partial T}{\partial r} = 0 \tag{4.22}$$

$$Q(Y_{i\infty} - Y_{is}) - D\rho \frac{\partial Y_i}{\partial r} = 0$$
(4.23)

Boundary conditions are considered between 0<r<rs.

The variables used for equations are extracted from Dasappa et al. [117] and summarized in Table 4.7.

Table 4.7: Parameters used in equations and their values [117]

Parameters	Sources
Gas phase density, kg/m3	Calculate w mass conservation equation
P	2
Sensity of non-porous wood char, kg/m3	1900 kg/m^3
ρ _c Calorific value of carbon	22.6 MI/lea
H _c	32.6 MJ/kg
Enthalpy of carbon (summation of C+CO ₂ ,	
C+O ₂ and C+H ₂ O reactions)	
Pore radius	(t=0)= 50 μm
r _p	1.5
Tortuosity factor T	1.5
Non-porous char thermal conductivity	1.85 W/m-K
K _c	1.05 W/III-K
Gas thermal conductivity	0.071 W/m-K
$ m K_g$	is calculated considering the presence of
	H_2 .
Porous char conductivity	0.4–0.5
	Temperature based. A volumetric average
	of gas and char conductivity
Unreacted char porosity	0.88
3	
Specific heat, kJ/(kg K)	1.25 KJ/kg
C_p	
Effective diffusivity	
D_{e}	In porous media is defined as follow:
	$\frac{D\epsilon_t\delta}{ au}$
	D is the diffusion coefficient in gas or
	liquid filling the pores

4. 3. Results and discussion

The numerical solution for the temperature distribution in 1D wood-char pellet has been calculated. To understand the result better, the profile has been divided into two graphs for the change of the radius while time is fixed, and the temperature change with the time while radius is fixed, both considering four different points for each fixed value.

Figure 4.1 demonstrates the change of the temperature as the radius increases for the 4 points from the start of time (0s) to finish (3000s). Due to the high infinity temperature, as the radius gets closer to the surface radius, temperature increases rapidly. This observation can be explained by the exposure to heat that is produced during the reactions and radiation received from the other particles. At the start of the gasification process, the difference between core temperature and the surface temperature is significantly high, creating strong heat conduction with a high rate of change. In addition, reactions have not reached stability thus the effect of heat of reaction is negligible at the start point. Both results can be observed by comparing the slope for the time at 300s and 3000s.

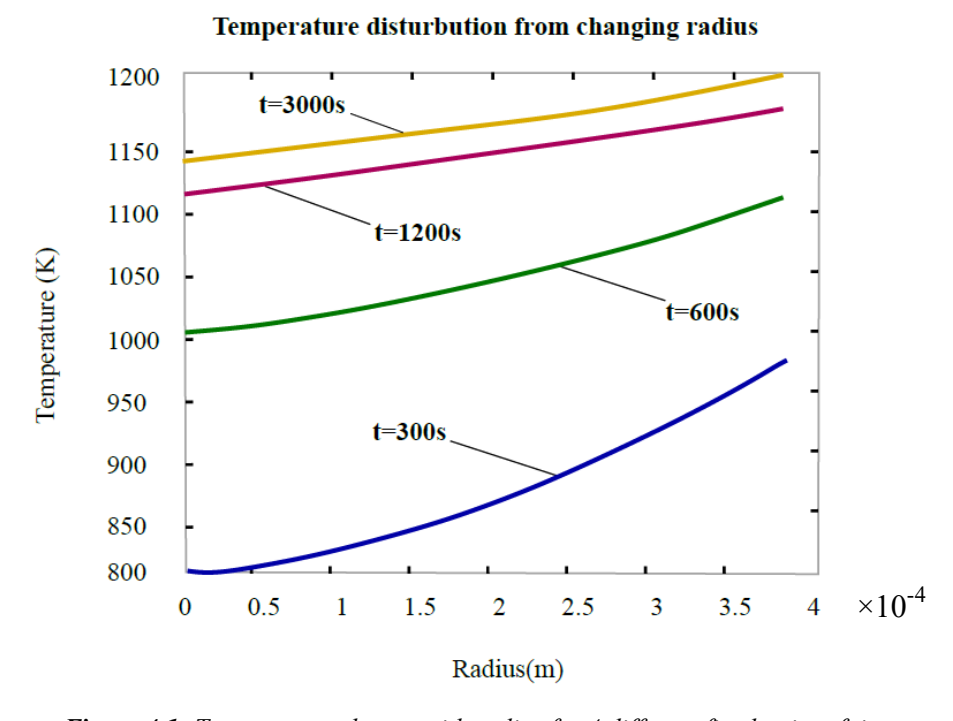


Figure 4.1: Temperature change with radius for 4 different fixed point of time

Moreover, as the process advances, the overall temperature of each radius goes higher by receiving heat and gets closer to the ambient temperature of 1200K, thus resulting in a smaller amount of heat conduction throughout the particle. As mentioned in chapter 2, based on Le Chatelier's principle, a higher value of temperature improves reactions such as Boudouard reaction, water—gas reaction, and steam-methane reforming reactions and thus enhancing gas yield. Therefore, as the reaction proceeds, the system gets closer to the steady state, thus maintaining the temperature with time. Finally, Figure 4.2 shows that although the slope has significantly decreased with time, the gradient of temperature still exists after 3000s and complete steady state has not been reached yet. These results emphasize on the accuracy of the model compare to simpler models such as equilibrium model since in the experiments equilibrium is almost never reached and considering steady state results in common imprecisions in the calculation of syngas components.

In Figure 4.2, the fixed and changing points have been replaced to study the effect of time on temperature. Figure 4.2 shows a more consistent trend with the different fixed points of radius, whereas the temperature rises rapidly at the start of the gasification and reaches a steady point near the end of time. This figure can be further used to determine the regimes of reaction based on the type of kinetic model considered (see section 2.5.2). High temperatures with steady trends that can be seen after t=2000s show a consistent state which eliminates the effect of temperature on the gas concentration, similar to an Arrhenius plot. Whereas between time 0s to 1000s, extreme change of temperature creates the regimes that are controlled either with chemical reaction or pore diffusion. The overall results show that the temperature of the particle reaches near steady-state while keeping a small gradient inside. The small gradient is due to the assumption of constant ambient temperature, which would require external heat for the reactor and is not a financially sustainable option.

The results of the modeling are in good agreement with the literature [90], thus making it applicable for testing the effect of changing properties such as effective thermal conductivity and porosity on the thermal distribution. Since temperature controls the mass transfer limitations, the temperature can be used as a source to determine the state of char reactions. However, due to the high number of assumptions, this model is only suitable for uncovering the trend changes, and thus the result values shall not be used directly.

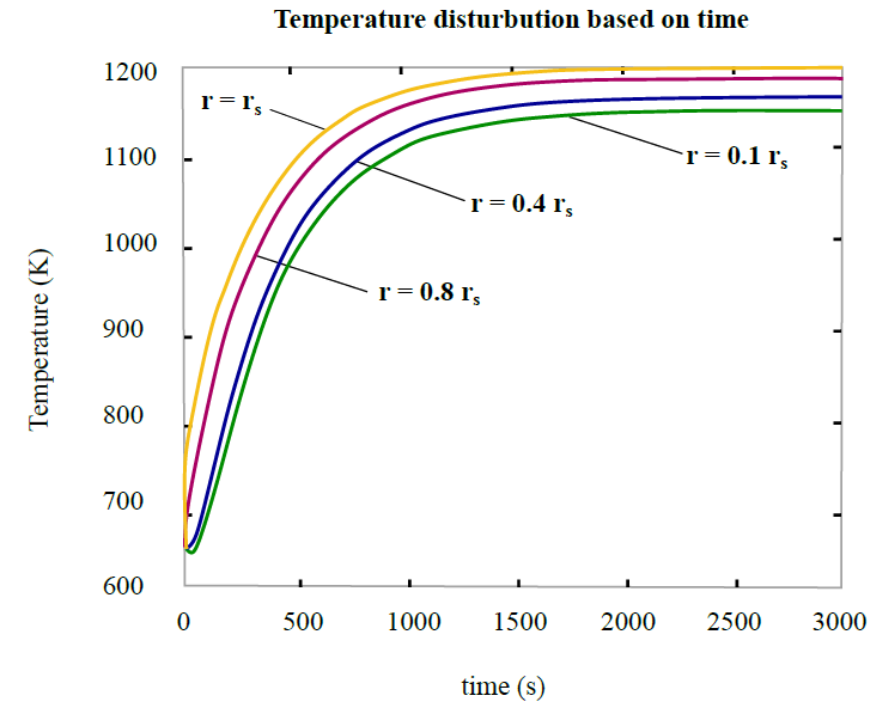


Figure 4.2: Temperature change with time at four different fixed point of radius

4. 4. Conclusions

A theoretical 1D model for transient gasification process of the biomass char in downdraft gasifier has been developed in this chapter. MATLAB in-built function *pdepe* was used for solving the parabolic equations. The purpose of this model was to create a simple tool for examining the change in the temperature profile with time and radius. The result was consistent with the trend of experimental data. The model can be used to determine temperature distribution of biomass during gasification by changing properties (e.g., porosity and thermal conductivity of particle). The presented model can be modified for 2D and 3D simulation of a whole bed in gasification of biomass char in a downdraft gasifier.

Chapter 5: Summary and recommendation for future studies

A thorough review of existing models for simulating gasification process based on the chemical equilibrium, kinetics, and heat transfer was conducted in Chapter 1, to provide the readers a background on the gasification process. Next, two numerical models targeting different aspects of the gasification process, namely the design of feedstock microstructure and process characterizations, were conducted. Using numerical homogenization model, implemented in this thesis, for calculating the effective thermal conductivity of the wood-plastic porous biocomposite is also a novel approach in the literature. However, there is a need for further investigation of the gasification process of the plastic itself, mainly due to the addition of the reactions to the set of known reactions for the gasification process. By studying the gasification process of WPCs and applying the necessary modification in the 1D numerical gasification model, the derived effective thermal conductivity can be used as an input for the gasification model to study the effect of using recycled WPC instead of wood as a feedstock. The choice of wood as a feedstock is because of the high rate of production of wood in Canada and the waste of by-products from this industry. However, wood is a seasonal product; as a result, the necessity to recycle plastics such as HDPE and having a better thermal conductivity of some plastic compared to porous wood, replacing wood with WPC can be considered as a more sustainable option. These simple models are beneficial and appealing in the preliminary study of a project, not to mention convincing the potential investors. This study has proven the competence of numerical modeling as a valuable tool in combination with the experiments for predicting the behavior of biomass in the complex processes of gasification.

5. 1. Recommendation for future studies

The possible recommendations are summarized as follow:

- Novel computational methods along with CFD modelling are required to be reviewed and compared with the heat transfer model [3, 111].
- Homogenization model can be modified to consider temperature-dependency of material constituents for determining the thermal conductivity of composite biomass [160]. The

- change of porosity can be considered by plotting the change of the effective thermal conductivity before and after the plastic inclusion in the matrix.
- Gasification model can be modified by considering 2D and 3D analysis similar to the model introduced by Bordbar et al.[105], which is a 3D coupled semi-empirical model of circulating fluidized bed and by adding the syngas composition calculations. The 3D result can be plotted against the effective thermal conductivity change of the feedstock using homogenization model. Another modification of the gasification model can be considered by studying the effect of gasifier type on gasification process.

References

- 1. Sansaniwal, S.K., M.A. Rosen, and S.K. Tyagi, *Global challenges in the sustainable development of biomass gasification: An overview.* Renewable and Sustainable Energy Reviews, 2017. **80**: p. 23-43.
- 2. Mainville, N., Fuelling a Biomess Greenpeace Canada, 2011.
- 3. Singh, R.I., A. Brink, and M. Hupa, *CFD modeling to study fluidized bed combustion and gasification*. Applied Thermal Engineering, 2013. **52**(2): p. 585-614.
- 4. Kumar, A., D.D. Jones, and M.A. Hanna, *Thermochemical biomass gasification: a review of the current status of the technology*. Energies, 2009. **2**(3): p. 556-581.
- 5. Basu, P., Chapter 7 Gasification Theory, in Biomass Gasification, Pyrolysis and Torrefaction (Second Edition). 2013, Academic Press: Boston. p. 199-248.
- 6. Sharma, S. and P.N. Sheth, *Air–steam biomass gasification: Experiments, modeling and simulation.* Energy Conversion and Management, 2016. **110**: p. 307-318.
- 7. Ismail, T.M. and M.A. El-Salam, *Parametric studies on biomass gasification process on updraft gasifier high temperature air gasification*. Applied Thermal Engineering, 2017. **112**: p. 1460-1473.
- 8. Baruah, D., D.C. Baruah, and M.K. Hazarika, *Artificial neural network based modeling of biomass gasification in fixed bed downdraft gasifiers*. Biomass and Bioenergy, 2017. **98**: p. 264-271.
- 9. Loha, C., H. Chattopadhyay, and P.K. Chatterjee, *Three dimensional kinetic modeling of fluidized bed biomass gasification*. Chemical Engineering Science, 2014. **109**(Supplement C): p. 53-64.
- 10. Baruah, D. and D.C. Baruah, *Modeling of biomass gasification: A review*. Renewable and Sustainable Energy Reviews, 2014. **39**: p. 806-815.
- 11. Materazzi, M., et al., *Thermodynamic modelling and evaluation of a two-stage thermal process for waste gasification*. Fuel, 2013. **108**: p. 356-369.
- 12. Siau, J.F., *Transport processes in wood*. 1984, Berlin; New York: Springer-Verlag.
- 13. Rupesh, S., C. Muraleedharan, and P. Arun, ASPEN plus modelling of air-steam gasification of biomass with sorbent enabled CO2 capture. Resource-Efficient Technologies, 2016. **2**(2): p. 94-103.
- 14. Gil, J., et al., *Biomass gasification in atmospheric and bubbling fluidized bed: Effect of the type of gasifying agent on the product distribution.* Biomass and Bioenergy, 1999. **17**(5): p. 389-403.
- 15. Ibrahimoglu, B., A. Cucen, and M.Z. Yilmazoglu, *Numerical modeling of a downdraft plasma gasification reactor*. International Journal of Hydrogen Energy, 2017. **42**(4): p. 2583-2591.
- 16. Susastriawan, A.A.P., H. Saptoadi, and Purnomo, *Small-scale downdraft gasifiers for biomass gasification: A review*. Renewable and Sustainable Energy Reviews, 2017. **76**(Supplement C): p. 989-1003.
- 17. Madadian, E., et al., Gasification of pelletized woody biomass using a downdraft reactor and impact of material bridging. Journal of Energy Engineering, 2016. **142**(4): p. 04016001.
- 18. Saravanakumar, A., T.M. Haridasan, and T.B. Reed, *Flaming pyrolysis model of the fixed bed cross draft long-stick wood gasifier*. Fuel Processing Technology, 2010. **91**(6): p. 669-675.

- 19. Pandey, D.S., et al., Multi-gene genetic programming based predictive models for municipal solid waste gasification in a fluidized bed gasifier. Bioresource Technology, 2015. 179: p. 524-533.
- 20. Kim, C.-O., et al., Dynamic modeling and simulation of reaction, slag ehavior, and heat transfer to water-cooling wall of shell entrained-flow gasifier. Vol. 33. 2016.
- 21. Phillips, J., Different types of gasifiers and their integration with gas turbines.
- 22. Roy, Y., et al., *Biomass combustion for greenhouse carbon dioxide enrichment*. Biomass and Bioenergy, 2014. **66**: p. 186-196.
- 23. Ruiz, J.A., et al., *Biomass gasification for electricity generation: Review of current technology barriers*. Renewable and Sustainable Energy Reviews, 2013. **18**(Supplement C): p. 174-183.
- 24. Mirmoshtaghi, G., et al., *The influence of different parameters on biomass gasification in circulating fluidized bed gasifiers*. Energy Conversion and Management, 2016. **126**: p. 110-123.
- 25. Madadian, E., A.H. Akbarzadeh, and M. Lefsrud, *Pelletized Composite Wood Fiber Mixed with Plastic as Advanced Solid Biofuels: Thermo-Chemical Analysis.* Waste and Biomass Valorization, 2017.
- 26. Madadian, E., et al., *Pelletized Composite Wood Fiber Mixed with Plastic as Advanced Solid Biofuels: Physico-Chemo-Mechanical Analysis.* Waste and Biomass Valorization, 2017.
- 27. Huo, W., et al., *Study on CO2 gasification reactivity and physical characteristics of biomass, petroleum coke and coal chars.* Bioresource Technology, 2014. **159**(Supplement C): p. 143-149.
- 28. Marques, A., et al., *Planning woody biomass supply in hot systems under variable chips energy content.* Biomass and Bioenergy, 2018. **108**: p. 265-277.
- 29. Rico-Contreras, J.O., et al., *Moisture content prediction in poultry litter using artificial intelligence techniques and Monte Carlo simulation to determine the economic yield from energy use.* Journal of Environmental Management, 2017. **202**: p. 254-267.
- 30. McKeown, M.S., et al., *Microwave sensing of moisture in flowing biomass pellets*. Biosystems Engineering, 2017. **155**: p. 152-160.
- 31. Xin, Y., et al., *Influence of moisture content on cattle manure char properties and its potential for hydrogen rich gas production*. Journal of Analytical and Applied Pyrolysis, 2018. **130**: p. 224-232.
- 32. Maxim, V., et al., Mathematical modeling and simulation of gasification processes with Carbon Capture and Storage (CCS) for energy vectors poly-generation, in Computer Aided Chemical Engineering, S. Pierucci and G.B. Ferraris, Editors. 2010, Elsevier. p. 697-702.
- 33. Jarungthammachote, S. and A. Dutta, *Thermodynamic equilibrium model and second law analysis of a downdraft waste gasifier*. Energy, 2007. **32**(9): p. 1660-1669.
- 34. Martínez-Lera, S. and J. Pallarés Ranz, On the development of a wood gasification modelling approach with special emphasis on primary devolatilization and tar formation and destruction phenomena. Energy, 2016. 113: p. 643-652.
- 35. Madadian, E., C. Crowe, and M. Lefsrud, *Evaluation of composite fiber-plastics biomass clinkering under the gasification conditions*. Journal of Cleaner Production, 2017. **164**: p. 137-145.

- 36. Madadian, E., V. Orsat, and M. Lefsrud, *Comparative Study of Temperature Impact on Air Gasification of Various Types of Biomass in a Research-Scale Down-draft Reactor*. Energy & Fuels, 2017. **31**(4): p. 4045-4053.
- 37. Sepe, A.M., J. Li, and M.C. Paul, *Assessing biomass steam gasification technologies using a multi-purpose model.* Energy Conversion and Management, 2016. **129**: p. 216-226.
- 38. Narobe, M., et al., Co-gasification of biomass and plastics: Pyrolysis kinetics studies, experiments on 100 kW dual fluidized bed pilot plant and development of thermodynamic equilibrium model and balances. Bioresource Technology, 2014. **162**: p. 21-29.
- 39. Zhang, W., *Automotive fuels from biomass via gasification*. Fuel Processing Technology, 2010. **91**(8): p. 866-876.
- 40. George, J., P. Arun, and C. Muraleedharan, *Stoichiometric Equilibrium Model Based Assessment of Hydrogen Generation through Biomass Gasification*. Procedia Technology, 2016. **25**(Supplement C): p. 982-989.
- 41. Rodriguez-Alejandro, D.A., et al., Development of a modified equilibrium model for biomass pilot-scale fluidized bed gasifier performance predictions. Energy, 2016. 115, Part 1: p. 1092-1108.
- 42. Masmoudi, M.A., et al., 2-D Modeling of thermo-kinetics coupled with heat and mass transfer in the reduction zone of a fixed bed downdraft biomass gasifier. Renewable Energy, 2014. 66: p. 288-298.
- 43. Ryu, C., et al., *Effect of fuel properties on biomass combustion: Part I. Experiments—fuel type, equivalence ratio and particle size.* Fuel, 2006. **85**(7–8): p. 1039-1046.
- 44. Dasappa, S., Thermochemical Conversion of Biomass, in Transformation of Biomass. 2014.
- 45. Levenspiel, O., Chemical reaction engineering. 1999, New York: Wiley.
- 46. Strange, J.F. and P.L. Walker, *Carbon-carbon dioxide reaction: Langmuir-Hinshelwood kinetics at intermediate pressures.* Carbon, 1976. **14**(6): p. 345-350.
- 47. Barrio, M. and J. Hustad, CO2 Gasification of Birch Char and the Effect of CO Inhibition on the Calculation of Chemical Kinetics. 2008. 47-60.
- 48. BiofuelNet, Advanced biofuels course.
- 49. FAO, The State of Food Insecurity in the World FAO statics, 2004.
- 50. Aguilar, F., H.E. Garrett, and Gene, *Perspectives of Woody Biomass for Energy: Survey of State Foresters, State Energy Biomass Contacts, and National Council of Forestry Association Executives.* Journal of Forestry, 2009. **107**(6): p. 297-306.
- 51. Mahapatra, S., S. Kumar, and S. Dasappa, *Gasification of wood particles in a co-current packed bed: Experiments and model analysis.* Fuel Processing Technology, 2016. **145**: p. 76-89.
- 52. Wu, X., J. Tang, and J. Wang, *A new active site/intermediate kinetic model for K2CO3-catalyzed steam gasification of ash-free coal char.* Fuel, 2016. **165**: p. 59-67.
- 73. Ross, A.B., et al., *Classification of macroalgae as fuel and its thermochemical behaviour.* Bioresource Technology, 2008. **99**(14): p. 6494-6504.
- 54. Dogru, M., A. Midilli, and C.R. Howarth, *Gasification of sewage sludge using a throated downdraft gasifier and uncertainty analysis.* Fuel Processing Technology, 2002. **75**(1): p. 55-82.
- 55. Ben Hassen-Trabelsi, A., et al., *Pyrolysis of waste animal fats in a fixed-bed reactor: Production and characterization of bio-oil and bio-char.* Waste Management, 2014. **34**(1): p. 210-218.

- 56. Kumar, A., et al., *Thermogravimetric characterization of corn stover as gasification and pyrolysis feedstock.* Biomass and Bioenergy, 2008. **32**(5): p. 460-467.
- 57. The state of Canada's forests: Annual report. 2017: Ottawa, CA.
- 58. Svishchev, D.A., et al., A semi-empirical approach to the thermodynamic analysis of downdraft gasification. Fuel, 2016. **168**(Supplement C): p. 91-106.
- 59. G., H.-O. and O. S., *The Fischer-Tropsch Synthesis: Molecular Weight Distribution of Primary Products and Reaction Mechanism.* Angewandte Chemie International Edition in English, 1976. **15**(3): p. 136-141.
- 60. Chang, C.D., *Hydrocarbons from Methanol*. Catalysis Reviews, 1983. **25**(1): p. 1-118.
- 61. Lin, C.-Y. and C.-C. Chiu, *Burning characteristics of palm-oil biodiesel under long-term storage conditions*. Energy Conversion and Management, 2010. **51**(7): p. 1464-1467.
- 62. 06/01982 Biomass resources present in Japan annual quantities grown, unused and wasted: Minami, E. and Saka, S. Biomass and Bioenergy, 2005, 29, (5), 310–320. Fuel and Energy Abstracts, 2006. 47(4): p. 298.
- 63. Carroll, A. and C. Somerville, *Cellulosic Biofuels*. Annual Review of Plant Biology, 2009. **60**(1): p. 165-182.
- 64. Antonopoulos, I.S., et al., *Modelling of a downdraft gasifier fed by agricultural residues*. Waste Management, 2012. **32**(4): p. 710-718.
- 65. La Villetta, M., M. Costa, and N. Massarotti, *Modelling approaches to biomass gasification: A review with emphasis on the stoichiometric method.* Renewable and Sustainable Energy Reviews, 2017. **74**(Supplement C): p. 71-88.
- 66. Shayan, E., V. Zare, and I. Mirzaee, *Hydrogen production from biomass gasification; a theoretical comparison of using different gasification agents*. Energy Conversion and Management, 2018. **159**: p. 30-41.
- 67. Patra, T.K. and P.N. Sheth, *Biomass gasification models for downdraft gasifier: A state-of-the-art review.* Renewable and Sustainable Energy Reviews, 2015. **50**: p. 583-593.
- 68. Shabbar, S. and I. Janajreh, *Thermodynamic equilibrium analysis of coal gasification using Gibbs energy minimization method.* Energy Conversion and Management, 2013. **65**: p. 755-763.
- 69. Altafini, C.R., P.R. Wander, and R.M. Barreto, *Prediction of the working parameters of a wood waste gasifier through an equilibrium model.* Energy Conversion and Management, 2003. **44**(17): p. 2763-2777.
- 70. Lim, Y.-i. and U.-D. Lee, *Quasi-equilibrium thermodynamic model with empirical equations for air-steam biomass gasification in fluidized-beds*. Fuel Processing Technology, 2014. **128**(Supplement C): p. 199-210.
- 71. Huang, H.-J. and S. Ramaswamy, *Modeling Biomass Gasification Using Thermodynamic Equilibrium Approach*. Applied Biochemistry and Biotechnology, 2009. **154**(1): p. 14-25.
- 72. Sanlisoy, A. and M.O. Carpinlioglu, *A review on plasma gasification for solid waste disposal*. International Journal of Hydrogen Energy, 2017. **42**(2): p. 1361-1365.
- 73. Materazzi, M., et al., Reforming of tars and organic sulphur compounds in a plasma-assisted process for waste gasification. Fuel Processing Technology, 2015. 137: p. 259-268.
- 74. Madadian, E., Experimental Observation on Downdraft Gasification for Different Biomass Feedstocks, in Gasification for Low-grade Feedstock. 2018, IntechOpen.

- 75. Cortazar, M., et al., *Role of temperature on gasification performance and tar composition in a fountain enhanced conical spouted bed reactor.* Energy conversion and management, 2018. **171**: p. 1589-1597.
- 76. Heidenreich, S. and P.U. Foscolo, *New concepts in biomass gasification*. Progress in Energy and Combustion Science, 2015. **46**(Supplement C): p. 72-95.
- 77. Surov, A.V., et al., *Multi-gas AC plasma torches for gasification of organic substances*. Fuel, 2017. **203**(Supplement C): p. 1007-1014.
- 78. Rutberg, P.G., et al., *On efficiency of plasma gasification of wood residues*. Biomass and Bioenergy, 2011. **35**(1): p. 495-504.
- 79. Yoon, S.J., et al., *Hydrogen and syngas production from glycerol through microwave plasma gasification*. International Journal of Hydrogen Energy, 2013. **38**(34): p. 14559-14567.
- 80. Hlina, M., et al., *Production of high quality syngas from argon/water plasma gasification of biomass and waste.* Waste Management, 2014. **34**(1): p. 63-66.
- 81. Du, C., et al., *Gasification of corn cob using non-thermal arc plasma*. International Journal of Hydrogen Energy, 2015. **40**(37): p. 12634-12649.
- 82. Cho, I.J., et al., *Enhancement of synthesis gas production using gasification-plasma hybrid system.* International Journal of Hydrogen Energy, 2015. **40**(4): p. 1709-1716.
- 83. Babu, B.V. and A.S. Chaurasia, *Heat transfer and kinetics in the pyrolysis of shrinking biomass particle*. Chemical Engineering Science, 2004. **59**(10): p. 1999-2012.
- 84. Lopez, G., et al., Assessment of steam gasification kinetics of the char from lignocellulosic biomass in a conical spouted bed reactor. Energy, 2016. **107**: p. 493-501.
- 85. Tremel, A. and H. Spliethoff, Gasification kinetics during entrained flow gasification Part III: Modelling and optimisation of entrained flow gasifiers. Fuel, 2013. **107**(Supplement C): p. 170-182.
- 86. Shie, J.-L., F.-J. Tsou, and K.-L. Lin, *Steam plasmatron gasification of distillers grains residue from ethanol production*. Bioresource Technology, 2010. **101**(14): p. 5571-5577.
- 87. Adeyemi, I. and I. Janajreh, *Modeling of the entrained flow gasification: Kinetics-based ASPEN Plus model.* Renewable Energy, 2015. **82**(Supplement C): p. 77-84.
- 88. Yu, J.L., et al., *A mechanistic study on char structure evolution during coal devolatilization—Experiments and model predictions.* Proceedings of the Combustion Institute, 2002. **29**(1): p. 467-473.
- 89. Kramb, J., et al., *Modeling biomass char gasification kinetics for improving prediction of carbon conversion in a fluidized bed gasifier.* Fuel, 2014. **132**(Supplement C): p. 107-115.
- 90. Kumar, S. and S. Dasappa, *Modeling and analysis of single particle conversion of biomass in a packed bed gasification system.* Applied Thermal Engineering, 2017. **112**: p. 1382-1395.
- 91. Akbarzadeh, A.H., et al., *Electrically conducting sandwich cylinder with a planar lattice core under prescribed eigenstrain and magnetic field.* Composite Structures, 2016. **153**: p. 632-644.
- 92. Zhou, C. and W. Yang, *Effect of heat transfer model on the prediction of refuse-derived fuel pyrolysis process.* Fuel, 2015. **142**(Supplement C): p. 46-57.
- 93. Ranzi, E., et al., *Kinetic modeling of the thermal degradation and combustion of biomass*. Chemical Engineering Science, 2014. **110**(Supplement C): p. 2-12.
- 94. Fernando, N. and M. Narayana, *A comprehensive two dimensional Computational Fluid Dynamics model for an updraft biomass gasifier*. Renewable Energy, 2016. **99**: p. 698-710.

- 95. Ismail, T.M., et al., Fluid dynamics model on fluidized bed gasifier using agro-industrial biomass as fuel. Waste Management, 2018. **73**: p. 476-486.
- 96. Gerber, S., F. Behrendt, and M. Oevermann, *An Eulerian modeling approach of wood gasification in a bubbling fluidized bed reactor using char as bed material.* Fuel, 2010. **89**(10): p. 2903-2917.
- 97. González, W.A., et al., *Numerical analysis of wood biomass packing factor in a fixed-bed gasification process.* Renewable Energy, 2018. **121**: p. 579-589.
- 98. Xue, Q. and R.O. Fox, Reprint of: Multi-fluid CFD modeling of biomass gasification in polydisperse fluidized-bed gasifiers. Powder Technology, 2014. **265**: p. 23-34.
- 99. Fox, R.O., CFD Models for Analysis and Design of Chemical Reactors, in Advances in Chemical Engineering, G.B. Marin, Editor. 2006, Academic Press. p. 231-305.
- 100. Silva, V. and A. Rouboa, Combining a 2-D multiphase CFD model with a Response Surface Methodology to optimize the gasification of Portuguese biomasses. Energy Conversion and Management, 2015. **99**: p. 28-40.
- 101. Su, M., H. Zhao, and J. Ma, Computational fluid dynamics simulation for chemical looping combustion of coal in a dual circulation fluidized bed. Energy Conversion and Management, 2015. **105**: p. 1-12.
- 102. Oevermann, M., S. Gerber, and F. Behrendt, *Euler–Lagrange/DEM simulation of wood gasification in a bubbling fluidized bed reactor.* Particulogy, 2009. **7**(4): p. 307-316.
- 103. Snider, D.M., S.M. Clark, and P.J. O'Rourke, Eulerian-Lagrangian method for three-dimensional thermal reacting flow with application to coal gasifiers. Chemical Engineering Science, 2011. **66**(6): p. 1285-1295.
- 104. Kapfunde, N., C.M. Masuku, and D. Hildebrandt, *Optimization of the Thermal Efficiency of a Fixed-Bed Gasifier using Computational Fluid Dynamics*, in *Computer Aided Chemical Engineering*, M.R. Eden, M.G. Ierapetritou, and G.P. Towler, Editors. 2018, Elsevier. p. 1747-1752.
- 105. Bordbar, H., K. Myöhänen, and T. Hyppänen, *Coupling of a radiative heat transfer model and a three-dimensional combustion model for a circulating fluidized bed furnace*. Vol. 76. 2014. 344–356.
- 106. Gogoi, B. and D.C. Baruah, *Steady state heat transfer modeling of solid fuel biomass stove: Part 1.* EGY Energy, 2016. **97**: p. 283-295.
- 107. Imomov, S.Z., *Heat transfer process during phase back-and-forth motion with biomass pulse loading.* Appl. Sol. Energy Applied Solar Energy, 2009. **45**(2): p. 116-119.
- 108. Jacobsen, S.E. and C.E. Wyman, *Heat transfer considerations in design of a batch tube reactor for biomass hydrolysis*. Applied biochemistry and biotechnology, 2001. **91-93**: p. 91-93.
- 109. Koufopanos, C.A., et al., *Modelling of the pyrolysis of biomass particles. Studies on kinetics, thermal and heat transfer effects.* CJCE The Canadian Journal of Chemical Engineering, 1991. **69**(4): p. 907-915.
- 110. Kumar, U. and V.K. Agarwal, *Biomass gasification in a fluidized bed reactor: Hydrodynamics and heat transfer studies.* Numerical Heat Transfer, Part A: Applications, 2016. **70**(5): p. 513-531.
- 111. Loha, C., et al., *Advances in mathematical modeling of fluidized bed gasification*. Renewable and Sustainable Energy Reviews, 2014. **40**: p. 688-715.

- 112. Perkins, G. and V. Sahajwalla, *Modelling of Heat and Mass Transport Phenomena and Chemical Reaction in Underground Coal Gasification*. Chemical Engineering Research and Design, 2007. **85**(3): p. 329-343.
- 113. Schulze, S., et al., *Heat and mass transfer within thermogravimetric analyser: From simulation to improved estimation of kinetic data for char gasification.* Fuel, 2017. **187**(Supplement C): p. 338-348.
- 114. Vargas, J.V.C., et al., *Mass transfer modeling and maximization of hydrogen rhythmic production from genetically modified microalgae biomass*. International Journal of Heat and Mass Transfer, 2016. **101**: p. 1-9.
- 115. Wiggins, G.M., P.N. Ciesielski, and C.S. Daw, *Low-Order Modeling of Internal Heat Transfer in Biomass Particle Pyrolysis*. Energy and fuels, 2016. **30**(6): p. 4960-4969.
- 116. Yrjölä, J., J. Paavilainen, and M. Sillanpää, *Modelling and experimental studies on heat transfer in the convection section of a biomass boiler*. ER International Journal of Energy Research, 2006. **30**(12): p. 939-953.
- 117. Dasappa, S., et al., *Wood-char gasification: Experiments and analysis on single particles and packed beds.* Symposium (International) on Combustion, 1998. **27**(1): p. 1335-1342.
- 118. Lu, X. and T. Wang, *Investigation of radiation models in entrained-flow coal gasification simulation*. International Journal of Heat and Mass Transfer, 2013. **67**: p. 377-392.
- 119. Yu, X., et al., CFD and experimental studies on a circulating fluidised bed reactor for biomass gasification. Chemical Engineering and Processing Process Intensification, 2018. 130: p. 284-295.
- 120. Pérez, J.F., P.N. Benjumea, and A. Melgar, Sensitivity analysis of a biomass gasification model in fixed bed downdraft reactors: Effect of model and process parameters on reaction front. Biomass and Bioenergy, 2015. **83**: p. 403-421.
- 121. Martinek, J., C. Bingham, and A.W. Weimer, Computational modeling and on-sun model validation for a multiple tube solar reactor with specularly reflective cavity walls. Part 1: Heat transfer model. Chemical Engineering Science, 2012. 81(Supplement C): p. 298-310.
- 122. Jiang, H. and D.P. Kamdem, *Development of poly(vinyl chloride)/wood composites*. *A literature review*. Journal of Vinyl and Additive Technology, 2004. **10**(2): p. 59-69.
- 123. Yam, K.L., et al., Composites from compounding wood fibers with recycled high density polyethylene. Polymer Engineering & Science, 1990. **30**(11): p. 693-699.
- 124. Părpăriță, E., et al., *TG/FT–IR/MS study on thermal decomposition of polypropylene/biomass composites*. Polymer Degradation and Stability, 2014. **109**: p. 13-20.
- 125. Sharypov, V.I., et al., *Co-pyrolysis of wood biomass and synthetic polymer mixtures. Part I: influence of experimental conditions on the evolution of solids, liquids and gases.* Journal of Analytical and Applied Pyrolysis, 2002. **64**(1): p. 15-28.
- 126. Ruoppolo, G., et al., *H2-rich syngas production by fluidized bed gasification of biomass and plastic fuel.* Waste Management, 2012. **32**(4): p. 724-732.
- 127. Mastellone, M.L., L. Zaccariello, and U. Arena, *Co-gasification of coal, plastic waste and wood in a bubbling fluidized bed reactor.* Fuel, 2010. **89**(10): p. 2991-3000.
- 128. Kim, J.K. and K. Pal, *Flammability in WPC Composites*, in *Recent Advances in the Processing of Wood-Plastic Composites*, J.K. Kim and K. Pal, Editors. 2011, Springer Berlin Heidelberg: Berlin, Heidelberg. p. 129-147.
- 129. Lopez, G., et al., *Effect of polyethylene co-feeding in the steam gasification of biomass in a conical spouted bed reactor.* Fuel, 2015. **153**: p. 393-401.

- 130. Di Blasi, C., *Influences of physical properties on biomass devolatilization characteristics*. Fuel, 1997. **76**(10): p. 957-964.
- 131. Suleiman, B.M., et al., *Thermal conductivity and diffusivity of wood*. Wood Science and Technology, 1999. **33**(6): p. 465-473.
- 132. Wurzenberger, J.C., et al., *Thermal conversion of biomass: Comprehensive reactor and particle modeling.* AIChE Journal, 2004. **48**(10): p. 2398-2411.
- 133. Babu, B.V. and A.S. Chaurasia, *Parametric study of thermal and thermodynamic properties on pyrolysis of biomass in thermally thick regime*. Energy Conversion and Management, 2004. **45**(1): p. 53-72.
- 134. Guo, W., et al., *Determination of effective thermal conductivity and specific heat capacity of wood pellets.* Fuel, 2013. **103**: p. 347-355.
- 135. Sova, D., et al., *Effective thermal conductivity models applied to wood briquettes*. International Journal of Thermal Sciences, 2018. **124**: p. 1-12.
- 136. Shebani, A.N., A.J. Van Reenen, and M. Meincken, *The Effect of Wood Species on the Mechanical and Thermal Properties of Wood—LLDPE Composites*. Journal of Composite Materials, 2009. **43**(11): p. 1305-1318.
- 137. Khan, M.A., K.M. Idriss Ali, and M.S. Rahman, *Swelling and Thermal Conductivity of Wood and Wood-Plastic Composite*. Polymer-Plastics Technology and Engineering, 1997. **36**(2): p. 179-187.
- 138. Thunman, H. and B. Leckner, *Thermal conductivity of wood—models for different stages of combustion*. Biomass and Bioenergy, 2002. **23**(1): p. 47-54.
- 139. Prisco, U., Thermal conductivity of flat-pressed wood plastic composites at different temperatures and filler content, in Science and Engineering of Composite Materials. 2014. p. 197.
- 140. Kumlutas, D. and I.H. Tavman, A Numerical and Experimental Study on Thermal Conductivity of Particle Filled Polymer Composites. Journal of Thermoplastic Composite Materials, 2006. **19**(4): p. 441-455.
- 141. Brenci, L.-M., et al., *Thermal Conductivity of Wood with ABS Waste Core Sandwich Composites Subject to Various Core Modifications*. BioResources, 2018. **13**(1): p. 555-568.
- 142. Chen, H., et al., *Thermal conductivity of polymer-based composites: Fundamentals and applications.* Progress in Polymer Science, 2016. **59**: p. 41-85.
- 143. Li, J., J. Gong, and S.I. Stoliarov, *Development of pyrolysis models for charring polymers*. Polymer Degradation and Stability, 2015. **115**: p. 138-152.
- 144. Agoua, E., et al., *Thermal conductivity of composites made of wastes of wood and expanded polystyrene*. Construction and Building Materials, 2013. **41**: p. 557-562.
- 145. Ndiaye, D., et al., *Thermal and mechanical properties of polypropylene/wood-flour composites*. Journal of Applied Polymer Science, 2010. **119**(6): p. 3321-3328.
- 146. Das, O., et al., Characterisation of waste derived biochar added biocomposites: chemical and thermal modifications. Science of The Total Environment, 2016. **550**: p. 133-142.
- 147. Anderson, C.E., D.E. Ketchum, and W.P. Mountain, *Thermal Conductivity of Intumescent Chars*. Journal of Fire Sciences, 1988. **6**(6): p. 390-410.
- 148. Maxwell, J.C., Art. 314. Medium in which small spheres are uniformly disseminated, Chapter IX. Conduction through heterogeneous media. A treatise on electricity and magnetism, 1873. 1: p. 365-366.

- 149. Rayleigh, L., LVI. On the influence of obstacles arranged in rectangular order upon the properties of a medium. The London, Edinburgh, and Dublin Philosophical Magazine and Journal of Science, 1892. **34**(211): p. 481-502.
- 150. Woodside, W., *CALCULATION OF THE THERMAL CONDUCTIVITY OF POROUS MEDIA*. Canadian Journal of Physics, 1958. **36**(7): p. 815-823.
- 151. Saastamoinen, J. and J.-R. Richard, *Simultaneous drying and pyrolysis of solid fuel particles*. Combustion and Flame, 1996. **106**(3): p. 288-300.
- 152. Aadmi, M., et al., *Effective thermal conductivity of random two-phase composites*. Journal of Reinforced Plastics and Composites, 2013. **33**(1): p. 69-80.
- 153. Zhao, J., et al., *Inverse determination of thermal conductivity in lumber based on genetic algorithms*, in *Holzforschung*. 2016. p. 235.
- 154. Rajeshwari, P. and T.K. Dey, Finite element modelling and experimental investigation on effective thermal conductivity of AlN (nano) particles reinforced HDPE polymer nanocomposites. Thermochimica Acta, 2016. **638**: p. 103-112.
- 155. Hunt, J.F. and H. Gu. Finite element analyses of two dimensional, anisotropic heat transfer in wood. in 2004 International ANSYS Conference: Pittsburgh, PA, May 24-26, 2004.[Sl: sn, 2004]: 13 pages. 2004.
- 156. Li, X., et al., Computational modeling and evaluation of the thermal behavior of randomly distributed single-walled carbon nanotube/polymer composites. Computational Materials Science, 2012. **63**: p. 207-213.
- 157. Ramani, K. and A. Vaidyanathan, *Finite Element Analysis of Effective Thermal Conductivity of Filled Polymeric Composites*. Journal of Composite Materials, 1995. **29**(13): p. 1725-1740.
- 158. Staggs, J.E.J., *Thermal conductivity estimates of intumescent chars by direct numerical simulation*. Fire Safety Journal, 2010. **45**(4): p. 228-237.
- 159. El Moumen, A., et al., Computational thermal conductivity in porous materials using homogenization techniques: Numerical and statistical approaches. Computational Materials Science, 2015. 97: p. 148-158.
- 160. Bourai, K., B. Riedl, and D. Rodrigue, *Effect of Temperature on the Thermal Conductivity of Wood-Plastic Composites*. Polymers & Polymer Composites, 2013. **21**(7).
- 161. Guedes, J. and N. Kikuchi, *Preprocessing and postprocessing for materials based on the homogenization method with adaptive finite element methods*. Computer Methods in Applied Mechanics and Engineering, 1990. **83**(2): p. 143-198.
- 162. Hollister, S.J. and N. Kikuchi, *A comparison of homogenization and standard mechanics analyses for periodic porous composites*. Computational Mechanics, 1992. **10**(2): p. 73-95.
- 163. Andreasen, E. and C.S. Andreasen, *How to determine composite material properties using numerical homogenization*. Computational Materials Science, 2014. **83**: p. 488-495.
- 164. Song, Y.S. and J.R. Youn, Evaluation of effective thermal conductivity for carbon nanotube/polymer composites using control volume finite element method. Carbon, 2006. 44(4): p. 710-717.
- 165. Shabana, Y.M. and N. Noda, *Numerical evaluation of the thermomechanical effective properties of a functionally graded material using the homogenization method.* International Journal of Solids and Structures, 2008. **45**(11): p. 3494-3506.

- 166. Dasgupta, A. and R.K. Agarwal, *Orthotropic Thermal Conductivity of Plain-Weave Fabric Composites Using a Homogenization Technique*. Journal of Composite Materials, 1992. **26**(18): p. 2736-2758.
- 167. Calonne, N., et al., *Numerical and experimental investigations of the effective thermal conductivity of snow.* Geophysical Research Letters, 2011. **38**(23).
- 168. Dasappa, S., et al. On the combustion of wood-char spheres in O2/N2mixtures— Experiments and analysis. in Symposium (International) on Combustion. 1994. Elsevier.
- 169. Howard, J.B. and R.H. Essenhigh, *Mechanism of solid-partical combustion with simultaneous gas-phase volatiles combustion*. Symposium (International) on Combustion, 1967. **11**(1): p. 399-408.
- 170. Semechkova, A. and D. Frank-Kamenetsky, *Recovering of dioxide by carbon*. Zh. Fiz. Khim, 1940. **14**(3): p. 291-304.
- 171. gases, U.I. *Air: its composition and properties*. Available from: http://www.uigi.com/air.html.